Healthcare; protein molecular weight standards from Bio-Rad; peanut agglutinin (PNA; biotinylated *Arachis hypogaea*) lectin and a series of lectin-conjugated agaroses from Seikagaku Corp.; Aβ40 from Peptide Institute; BCA protein assay reagents and sulfo-NHS-LC-biotin from Thermo Fisher Scientific; all other chemicals were from Sigma or Wako Chemicals. An anti-APP (C15) rabbit polyclonal antibody against endogenous membrane-bound (intact) APP was a generous gift from Dr. Kei Maruyama (Saitama Medical University, Saitama, Japan). The commercially available antibodies used were as follows: mouse monoclonal anti-APP 22C11 (Chemicon); anti-human sAPPα (6E10; Signet Laboratories); anti-GAPDH (Chemicon); anti-KPI (Chemicon); anti-OX2 (Chemicon); anti-human sAPPβ (IBL Co.); goat polyclonal anti-platelet endothelial cell adhesion molecule (Santa Cruz Biotechnology). The clinical study was approved by the Ethical Committee of RIKEN and Fukushima Medical University (No. 613). All animal experiments were performed in compliance with the institutional guidelines for animal experiments of RIKEN.

Expression Plasmids and Cell Culture—Human APP770 FLAG-pcDNA was constructed by inserting a human APP770 sequence generated by PCR (primers 1 and 2) at the SalI and HindIII sites of pcDNA, and a FLAG domain fragment was generated by annealing primers 3 and 4 at the HindIII and XbaI sites of pcDNA. A ViraPower Adenoviral Expression system (Invitrogen) was used to produce recombinant adenoviruses carrying human APP-FLAG, according to the manufacturer's protocol. A series of APP770-pcDNA3.1 mutants was generated using a QuikChange site-directed mutagenesis kit (Stratagene). To generate the APP_{OX2All} mutant, in which all of the possible *O*-glycosylation sites in the OX2 domain were deleted, $APP_{S346A,S348A}$ was constructed first, followed by creation of the APP_{OX2All} mutant using $APP_{S346A,S348A}$ as a template and the primers APP_{SOX2A} forward and reverse. To generate the APP_{all} mutant, in which all the reported *O*-glycosylation sites (16) in the whole APP770 region were deleted, we used the APP_{OX2all} mutant as a template and the primers $APP_{T366A,T367A}$ and APP_{T651A} to change Thr^{366}, Thr^{367}, and Thr^{651} to Ala. The primer information is shown in Table 1, *A* and *B*. Human BMECs (Applied Cell Biology Research Institute) were cultured in CS-C complete medium with or without FBS and used within four passages. Human umbilical vein endothelial cells (TaKaRa) were cultured in EMB-2 (TaKaRa) containing 2% FBS and EGM-2™ SingleQuots (TaKaRa) and used within four passages. Primary liver sinusoidal endothelial cells were prepared from mouse livers using CD146 MicroBeads (Miltenyi Biotech) according to the manufacturer's protocol (17). COS-7 cells were cultured in DMEM containing 10% FBS. Cortical neurons were isolated from C57BL/6CrSlc mice as described previously (18).

Patients and Samples—A patient (60 years of age) who died from a nonketotic hyperosmolar coma was recruited for this study. Cerebrospinal fluid (CSF) samples were collected from patients with AD.

PCR Analysis of APP Transcripts—Total RNA was isolated from cells using the Sepasol reagent (Nacalai Tesque, Inc.), and 5 μg of the isolated RNA was reverse-transcribed with random hexamers using a SuperScript III RT kit (Invitrogen) according to the manufacturer's protocol. The obtained cDNA samples were subjected to PCR analyses with primers A and D for APP695, APP751, and APP770, primers B and D for APP751 and APP770, and primers C and D for APP770. PCR was performed for 28 cycles (95 °C for 40 s, 56 °C for 40 s, and 72 °C for 90 s). The primer information is shown in Table 1*C*.

TABLE 1
Primers used in this study

A		Primers used to generate the human APP770 FLAG pcDNA
primer name		sequence
1	forward	GTCGACATGCTGCCCGGTTTGGCACTGC
2	reverse	AAGCTTGTTCTGCATCTGCTCAAAGAAC
3	forward	AGCTTGACTACAAGGACGACGATGACAAGTGAT
4	reverse	CTAGATCACTTGTCATCGTCGTCCTTGTAGTCA

B		Primer information used to generate the human APP770 mutants
A primer name		primer sequence
APP_{S346A}	forward	TGTGGCAGCGCCATGGCCCAAAGTTTACTCAAG
	reverse	CTTGAGTAAACTTTGGGCCATGGCGCTGCCACA
APP_{S348A}	forward	GCGCCATGTCCCAAGCCTTACTCAAGACTACCC
	reverse	GGGTAGTCTTGAGTAAGGCTTGGGACATGGCGC
$APPS_{T352A}$	forward	CCCAAAGTTTACTCAAGGCCACCCAGGAACCTC
	reverse	GAGGTTCCTGGGTGGCCTTGAGTAAACTTTGGG
APP_{T353A}	forward	ACTCAAGACTGCCCAGGAACCTCTTGC
	reverse	GCAAGAGGTTCCTGGGCAGTCTTGAGT
$APP_{S346,348A}$	forward	GCGCCATGGCCCAAGCCTTACTCAAGACTACCC
	reverse	GGGTAGTCTTGAGTAAGGCTTGGGCCATGGCGC
APP_{SOX2A}	forward	GTTTACTCAAGGCCGCCCAGGAACCTCTTGC
	reverse	GCAAGAGGTTCCTGGGCGGCCTTGAGTAAAC
$APP_{T291,292A}$	forward	TGTTAAACTTCCTGCAGCAGCAGCCAGTACCCC
	reverse	GGGGTACTGGCTGCTGCTGCAGGAAGTTTAACA
APP_{T651A}	forward	CGACCGAGGACTGGCCACTCGACCAGG
	reverse	CCTGGTCGAGTGGCCAGTCCTCGGTCG
APP_{S292A}	forward	CGAGAGGTGTGCGCCGAACAAGCCGAG
	reverse	CTCGGCTTGTTCGGGCGCACACCTCTCG
APP_{T297A}	forward	GAACAAGCCGAGGCCGGGCCGTGCCG
	reverse	CGGCACGGCCCGGCCTCGGCTTGTTC
APP_{S305A}	forward	CGAGCAATGATCGCCCGCTGGTACTTTG
	reverse	CAAAGTACCAGCGGGCGATCATTGCTCG
APP_{T312A}	forward	GGTACTTTGATGTGGCCGAAGGGAAGTGTGC
	reverse	GCACACTTCCCTTCGGCCACATCAAAGTACC
APP_{T333A}	forward	CGGAACAACTTTGACGCCGAAGAGTACTGCATG
	reverse	CATGCAGTACTCTTCGGCGTCAAAGTTGTTCCG
APP_{S343A}	forward	CCGTGTGTGGCGCCGCCATGTCCC
	reverse	GGGACATGGCGGCGCCACACACGG

C	Primers used to analyze the APP transcripts
primer name	sequence
A	ATGCTGCCCGGTTTGGCACTG
B	CGAGAGGTGTGCTCTGAACAAG
C	CCATGTCCCAAAGTTTACTCAAG
D	CTAGTTCTGCATCTGCTCAAAG

Immunohistochemistry—Brain tissue was fixed in phosphate-buffered 15% formalin solution and embedded in paraffin. A pair of serial sections (5-μm thick) was stained with hematoxylin and eosin or incubated with an anti-OX2 antibody (1:100) overnight at 37 °C followed by biotinylated anti-rabbit IgG (1:200). Bound antigens were visualized with the avidin and biotin-peroxidase complex method (ABC kit, Vector Laboratories).

APP Detection—Cell lysates were solubilized in T-PER buffer (Thermo Fischer Scientific, Inc.) containing a protease inhibitor mixture (Roche Applied Science). For lectin precipitation, BMEC lysates (0.1 mg of protein) were incubated with *Sambucus sieboldiana* agglutinin-, *Maackia amurensis* agglutinin-, PNA-, phytohemagglutinin-E4-, *Ricinus communis* agglutinin 120-, concanavalin A-, or jacalin-agarose (20 μl each) for 16 h. For APP immunoprecipitation, BMEC lysates

(0.25 mg of protein) were incubated with the anti-APP C15 antibody (5 μg) for 16 h. The precipitated samples were washed three times with T-PER buffer prior to SDS-PAGE analysis or sialidase treatment. Human CSF (0.2–0.5 ml) or media from cultured cells (0.5–1 ml) were incubated with heparin-Sepharose (Thermo Fisher Scientific). The precipitates were washed three times with PBS. The samples were then subjected to SDS-PAGE (5–20% gradient gel) and transferred to nitrocellulose membranes. For Western blot analyses, the membranes were incubated with anti-APP 22C11 (1:1000 dilution), anti-APP C15 (1:1000 dilution), anti-sAPPβ (1:500 dilution), anti-sAPPα (1:1000 dilution), anti-KPI (1:250 dilution), or anti-OX2 (1:250 dilution) antibodies. Appropriate horseradish peroxidase-conjugated donkey anti-goat IgG (Jackson ImmunoResearch Laboratories), anti-mouse, and anti-rabbit IgG (GE Healthcare) antibodies were used as the secondary antibodies (1:1,000 dilution). For lectin blot analyses, the membranes were incubated with PNA-biotin (1:100 dilution) and horseradish peroxidase-streptavidin (1:1000 dilution; GE Healthcare). A chemiluminescent substrate (Thermo Fisher Scientific) was used for detection of the bound antibodies. As a loading control, we detected GAPDH using the same membranes by incubation with an anti-GAPDH antibody (1:250 dilution; Chemicon). The detected signals were quantified with a luminoimage analyzer LAS-1000 PLUS (Fujifilm).

Aβ Quantification—BMECs were infected with adenovirus preparations for APP770-FLAG overexpression and cultured in Opti-MEM for 8 h. The levels of Aβ40 and Aβ42 in the media were determined using a human amyloid β(1–40) or (1–42) assay kit (IBL Co.) for BMECs and a human/rat β-amyloid(40) or (42) ELISA Kit (Wako Chemicals) for mouse neurons.

Glycosidase Digestion—Cell lysates, APP precipitates from cell lysates, culture media, and heparin-precipitated samples from culture media were incubated in the presence or absence of *Arthrobacter ureafaciens* sialidase (4 milliunits) and/or *O*-glycosidase (2 milliunits) for 18 h.

Cell Surface Biotinylation—BMECs grown in 10-cm culture plates were labeled with Sulfo-NHS-LC-Biotin for 30 min at 4 °C. After washing the plates three times with 0.1 M glycine in PBS (pH 8.0) and once with PBS, cell lysates were prepared. NHS-SS-biotin was used for internalization assays. After two washes with ice-cold PBS, the cells were cultured in pre-warmed CS-C media for 0 or 1 h at 37 °C. After washing once with ice-cold CS-C media and twice with PBS/10% FBS, the remaining cell surface biotin was removed by incubating the cells in buffer containing the nonpermeant reducing agent GSH (50 mM GSH, 75 mM NaCl, 0.3% NaOH, and 10% FBS) twice for 20 min each at 4 °C (19). After the reaction was quenched by 5 mg/ml of iodoacetamide in PBS containing 1% BSA, cell lysates were prepared. Biotinylated cell surface proteins were pulled down from the lysates with streptavidin-Sepharose (GE Healthcare) for further analysis.

Benzyl N-Acetyl Galactosamine (GalNAc) Treatment—Subconfluent BMECs grown on 10-cm tissue culture plates were incubated in the presence of benzyl GalNAc (2 mM) for 18 h, before cell lysates and culture media samples were prepared for further analysis.

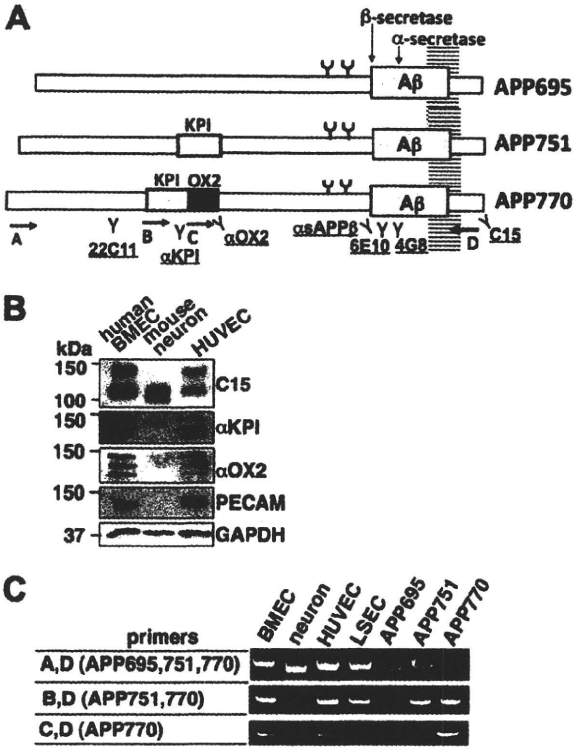

FIGURE 1. **Characterization of APP in brain endothelial cells.** *A*, schematic diagrams of the three alternatively spliced APP isoforms: APP695, APP751, and APP770. Compared with APP695, APP751 has an additional KPI domain, whereas APP770 has a KPI domain plus an OX2 domain. The recognition sites of a series of anti-APP antibodies and primers A, B, C, and D used to analyze the APP transcripts are shown. Two *N*-glycosylation sites are also shown. *B*, Western blot analysis of APP in cell lysates (20 μg of protein) from BMECs, mouse primary neurons and human umbilical vein endothelial cells using anti-APP C15, anti-KPI, anti-OX2, anti-platelet endothelial cell adhesion molecule (*PECAM*), and anti-GAPDH antibodies. *C*, total RNA was extracted from BMECs, neurons, human umbilical vein endothelial cells (*HUVEC*), and liver sinusoidal endothelial cells (*LSEC*), reverse-transcribed, and then subjected to PCR to detect the respective APP transcripts. APP695, APP751, and APP770 plasmids were used as standards.

RESULTS

Brain Endothelial Cells Express APP770—The human brain expresses three alternatively spliced APP mRNA isoforms: APP695, APP751, and APP770 (12, 13) (Fig. 1*A*), whereas neurons exhibit restricted expression of APP695 (14, 20, 21). This suggests that cell type-specific APP splicing events occur in the brain. In the present study, we focused on brain endothelial cells and established primary human BMECs to characterize the brain endothelial APP. Western blot analysis using an anti-APP C-terminal antibody (C15) showed that BMECs expressed equivalent or rather higher levels of APP compared with primary neurons (Fig. 1*B*). Interestingly, the endothelial APP exhibited two discrete bands, based on gel mobility after SDS-PAGE. Because the anti-KPI and anti-OX2 antibodies also detected these signals, we concluded that endothelial cells expressed APP770. Neither the anti-KPI nor the anti-OX2 antibodies detected neuronal APP, thereby confirming previous reports that neurons solely express APP695

(14, 20). When we analyzed BMEC lysates with the anti-KPI or anti-OX2 antibodies, we observed an additional band between the two APP bands. This additional band is most likely the processed form of APP, sAPP, which lacks the C-terminal sequence of APP. Using the OX2 antibody, we could detect APP770 in endothelial cells prepared from mouse brains (supplemental Fig. S1). Furthermore, human umbilical vein endothelial cells also expressed the two forms of APP, although their expression levels were significantly lower than those in BMECs (Fig. 1*B*), indicating that APP770 is broadly expressed in endothelial cells.

To analyze the APP transcripts, we isolated RNA from endothelial cells and primary neurons. Reverse-transcribed cDNA samples were then analyzed by PCR using a series of oligonucleotide primers to detect APP695, APP751, and APP770. The results confirmed the cell type-specific APP expression, as neurons expressed APP695, whereas endothelial cells expressed APP770 and not APP695 (Fig. 1*C*).

Endothelial APP770 Has Sialylated Core 1 Type O-Glycans—Because APP potentially has two *N*- and multiple *O*-glycans (16, 22, 23), we expected that the high molecular weight APP770 (APP-H) would be heavily glycosylated. We first performed glycosidase treatment, in which sialidase-treated and -untreated APP were incubated with PNGase. We found that the low molecular weight APP770 (APP-L) was resistant to sialidase treatment, indicating that APP-L contains no sialic acid (Fig. 2*A*). After PNGase treatment, both APP-H and APP-L moved slightly faster on SDS-PAGE gels, indicating that both forms contain *N*-glycan chains, although their molecular weight difference cannot be explained by *N*-glycans alone. Furthermore, the mobility difference between APP-H and de-*N*-glycosylated APP-H on SDS-PAGE gels was similar to that after sialidase treatment. This suggests that few sialic acids, if any, were present in the *N*-glycans of APP-H. Indeed, it seems that both APP-H and APP-L were sensitive to endoglycosidase H, which cleaves high mannose and some hybrid types of *N*-glycans (supplemental Fig. S2). After sialidase treatment, the mobility of APP-H shifted markedly and became closer to that of APP-L (Fig. 2, *A* and *B*). Similarly, after treatment with *O*-glycosidase, which only cleaves unsubstituted core 1 and 3 type *O*-glycans, the mobility of APP-H perfectly matched that of APP-L (Fig. 2*B*). We also found that sialidase-treated APP-H reacted with PNA lectin that specifically detects core 1 type *O*-glycans (Fig. 2*C*). Furthermore, a series of lectin pulldown assays showed that APP-H and APP-L have affinities for *Sambucus sieboldiana* agglutinin- and concanavalin A-lectin, respectively (Fig. 2*D*). In addition to the above results, judging from the fact that *Sambucus sieboldiana* agglutinin lectin recognizes Siaα2,6Gal/GalNAc, we concluded that APP-H has α2,6-sialylated core 1 type *O*-glycans.

When we overexpressed APP695, APP751, or APP770 in COS cells, mobility differences between the two APP forms were always clearly observed in the case of APP770 (Fig. 3*A*). These preliminary data suggested the presence of *O*-glycans in the OX2 domain. Therefore, we generated a series of APP770 mutants in which each Ser/Thr residue within the OX2 domain was individually changed to Ala (Fig. 3*B*). We

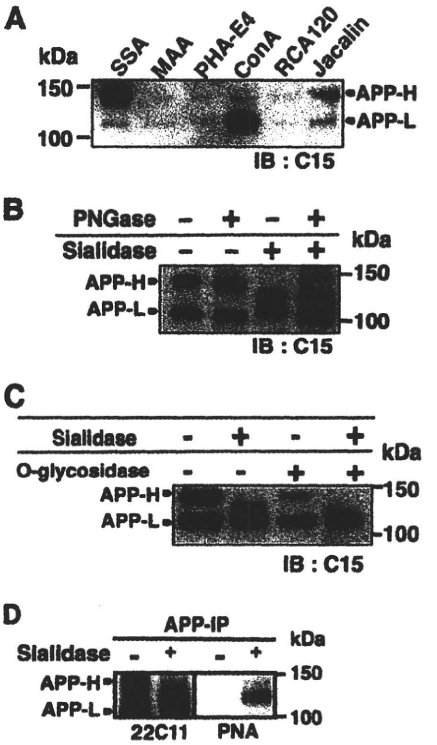

FIGURE 2. **Glycan analysis of brain endothelial APP.** *A*, BMEC lysates (20 μg of protein) were incubated in the presence or absence of PNGase and with or without sialidase. The digested samples were analyzed using the anti-APP C15 antibody. *B*, BMEC lysates (6 μg of protein) were incubated in the presence or absence of sialidase *O*-glycosidase and then immunostained with the anti-APP C15 antibody. *C*, APP precipitated from BMEC lysates (0.25 mg of protein) using the anti-APP C15 antibody (5 μg) was incubated in the presence or absence of sialidase (4 milliunits). The digested samples were subjected to Western blot analysis with the anti-APP 22C11 antibody or PNA lectin blot analysis. *D*, BMEC lysates (100 μg of protein) were incubated with *Sambucus sieboldiana* agglutinin (*SSA*)-, Maackia amurensis agglutinin (MAA)-, E4-phytohemagglutinin (*PHA-E4*)-, concanavalin A (*ConA*)-, *Ricinus communis* agglutinin (*RCA*)120-, or jacalin-agarose for 16 h at 4 °C. The lectin-precipitated samples were washed and analyzed by Western blotting with the anti-APP C15 antibody. *IB*, immunoblot.

then overexpressed wild-type APP770 and its mutants in COS cells. Even though the *O*-glycosylation machinery is not well developed in COS cells, we detected a lower level of APP-H (Fig. 3*C*). Mutations at Ser^{346}, Ser^{348}, and Thr^{352} had no effect on the mobility of the APP mutants on SDS-PAGE gels, whereas the APP_{T353A} mutant, in which Thr^{353} was changed to Ala, migrated faster than wild-type APP770 (Fig. 3, *B* and *C*). These results suggest that an *O*-glycan is attached to Thr^{353}. The findings that both APP_{T353A} and APP_{OX2all}, in which all of the Ser/Thr residues within the OX2 domain were mutated to Ala, still exhibited two discrete bands suggested the presence of additional *O*-glycosylation sites in domains other than the OX2 domain in APP770. Perdivara *et al.* (16) recently showed that APP695 is modified with *O*-glycans at Thr^{291}, Thr^{292}, and Thr^{576} (Thr^{366}, Thr^{367}, and Thr^{651} for APP770). Therefore, we next generated the APP770 mutant APP_{all}, in which Thr^{366}, Thr^{367}, Thr^{651}, and Thr^{652} were additionally changed to Ala from APP_{OX2all}. APP_{all} mostly showed a single band (Fig. 3*C*), indicating that we had mutated all of the *O*-glycosylation sites of APP770 in the APP_{all} mutant.

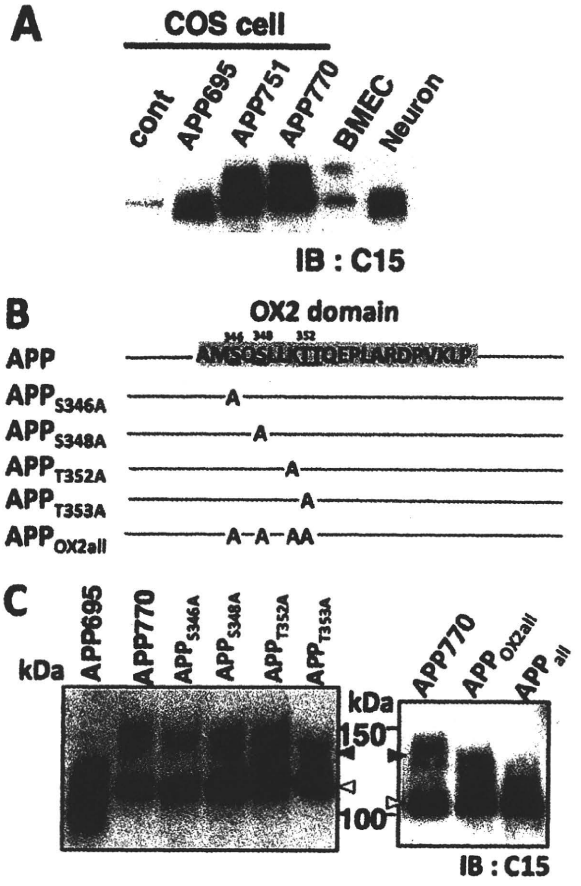

FIGURE 3. **Analysis of a series of APP770 mutants.** *A*, human APP695, APP751, and APP770 were individually overexpressed in COS cells. The obtained cell lysates (1 μg of protein) together with lysates of BMECs (5 μg of protein) and neurons (10 μg of protein) were analyzed by Western blotting with the anti-APP C15 antibody. *B*, schematic diagrams of the APP770 mutants used in this study. *C*, wild-type APP770 or its mutants were expressed in COS cells and subjected to Western blot analysis with the anti-APP C15 antibody. The *black* and *gray arrowheads* show APP-H and APP-L, respectively. *cont*, control; *IB*, immunoblot.

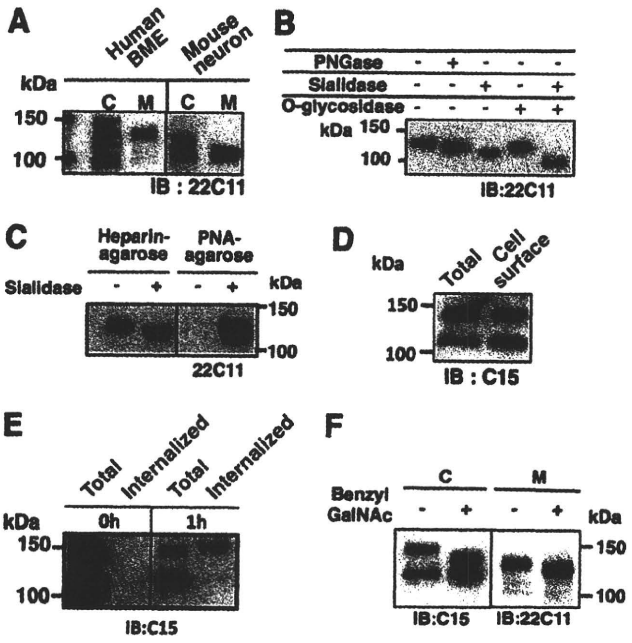

FIGURE 4. **Characterization of sAPP secreted from BMECs.** *A*, intact APP in cell lysates (6 μg) and soluble secreted sAPP pulled-down with heparin-agarose from the media of BMECs and mouse primary neurons were analyzed by Western blotting with the anti-APP 22C11 antibody. *C*, cell lysates; *M*, media. *B*, sAPP pulled down with heparin-agarose from the BMEC media was incubated in the presence or absence of sialidase and *O*-glycosidase and then analyzed by immunoblotting (*IB*) with the anti-APP 22C11 antibody. *C*, media from BMEC cultures (0.5 ml) were incubated in the presence or absence of *Arthrobacter ureafaciens* sialidase (4 milliunits) for 18 h. The digested samples were incubated with heparin-agarose or PNA agarose (20 μl each). The precipitated samples were analyzed by Western blotting with the anti-APP 22C11 antibody. *D*, following cell-surface biotinylation of BMECs, biotinylated cell surface proteins were precipitated with streptavidin-Sepharose and then analyzed by Western blotting with the anti-APP C15 antibody. *E*, after cell-surface labeling of BMECs using NHS-SS-biotin, the cells were incubated for 0 or 1 h to allow internalization of the biotinylated proteins. Cell surface biotin was then stripped by reductive treatment. Total proteins, or internalized biotinylated proteins that were precipitated with streptavidin-Sepharose, were analyzed by Western blotting with the anti-APP C15 antibody. *F*, BMECs were cultured in the presence of benzyl GalNAc, and then intact APP and sAPP were analyzed by Western blotting with the anti-APP C15 and 22C11 antibodies, respectively.

O-Glycosylated APP770 Is Preferentially Secreted to Media—Next, we analyzed the APP metabolites in endothelial cells. We performed Western blot analyses of BMEC lysates and culture media with the anti-APP 22C11 antibody, which recognizes the N-terminal APP region and therefore detects sAPP. We observed three bands in the cell lysates using the anti-22C11 antibody. In the media, we detected a single sAPP band that migrated with the middle band observed in the cell lysates (Fig. 4*A*), suggesting that sAPP is solely derived from APP-H. Indeed, sAPP was sensitive to both sialidase and *O*-glycosidase treatments (Fig. 4*B*). Furthermore, after sialidase treatment, most of the sAPP was precipitated with PNA lectin (Fig. 4*C*), indicating that sAPP mostly contains sialylated core 1 type *O*-glycan chains. It should be noted that we failed to detect sAPP without *O*-glycans. Considering that APP cleavage at the α-site seems to occur at the cell surface, whereas cleavage at the β-site occurs during the endocytotic pathway (24), it is possible that APP without *O*-glycosylation is unable to move to the cell surface to encounter either α- or β-secretase. However, cell surface biotinylation experiments showed that both APP-H and APP-L reached the cell surface (Fig. 4*D*). We next studied how cell surface APP is metabolized in the cell. To analyze APP internalization, we next labeled the surface of BMECs with a disulfide cleavable biotinylation reagent (19). Internalization was then induced at 37 °C for 1 h. Interestingly, we found that only APP-H was endocytosed (Fig. 4*E*). This suggests that cell surface APP-H uses a specific intracellular trafficking pathway to encounter both α- and β-secretase. Furthermore, benzyl GalNAc, an inhibitor of *O*-glycan chain elongation, failed to inhibit sAPP secretion into the media (Fig. 4*F*).

Aβ is Produced from Brain Endothelial Cells—Since there is limited information regarding the expression levels and activities of the endothelial α-secretase and β-secretase enzymes for the processing of APP770, we characterized the soluble sAPP770 secreted from BMECs. Using specific antibodies against sAPPα and sAPPβ, we successfully detected both sAPP770α and sAPP770β (Fig. 5*A*). Since the amyloidogenic β-secretase pathway is present in endothelial cells, it is rea-

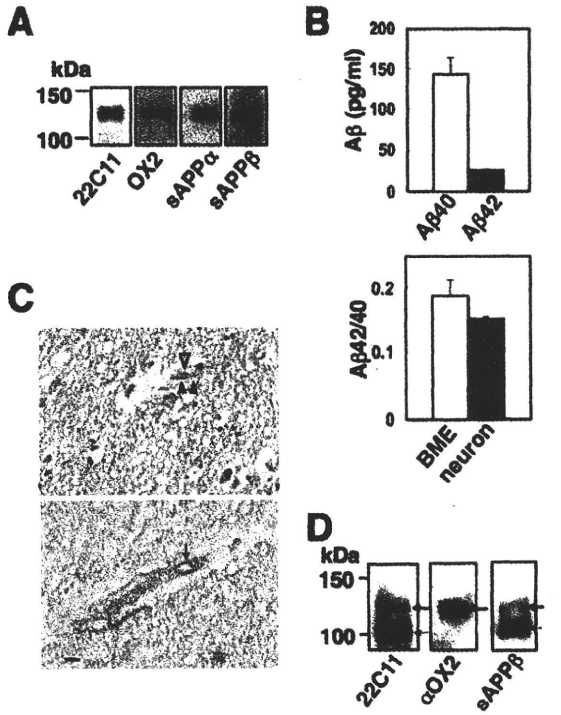

FIGURE 5. **Analysis of APP770 in the human brain.** *A*, sAPP770 secreted from BMECs was analyzed by Western blotting with anti-APP 22C1, anti-OX2, anti-sAPPα, and anti-sAPPβ antibodies. *B*, culture media from BMECs cultured in Opti-MEM were analyzed for their levels of Aβ40 and Aβ42 (n = 3; *upper panel*). The ratios of Aβ42/Aβ40 secreted from BMECs and neurons are shown as the means ± S.E. (n = 4) (*lower panel*). *C*, paraffin-embedded human cerebral sections were analyzed by hematoxylin-eosin staining (*upper panel*) and immunostaining with the anti-OX2 antibody (*lower panel*). The *gray* and *black arrowheads* show the nuclei of endothelial cells and smooth muscle cells, respectively. The *arrow* shows the OX2-immunoreactive endothelium. *Scale bar*, 20 μm. *D*, sAPP in human CSF samples (0.5 ml each) was pulled down with heparin-agarose (30 μl) and then analyzed by Western blotting with anti-APP 22C11, anti-sAPPβ, and anti-OX2 antibodies.

sonable to consider that these cells also have γ-secretase activity to produce Aβ peptides. Even though endogenous Aβ was not detectable, we detected both Aβ40 and Aβ42 in the culture media of BMECs overexpressing APP770, and the ratio of endothelial Aβ42/Aβ40 was similar to that in neurons (Fig. 5*B*).

APP770 is Expressed in Cerebral Vessels and sAPP770β Is Secreted into the CSF—To clarify whether APP770 is indeed expressed in cerebral vessels, we first analyzed cerebral cortex sections with an anti-OX2 antibody to determine the localization of APP770. The luminal regions of the venous and venular endothelial cells, but not smooth muscle cells, were stained with the anti-OX2 antibody (Fig. 5*C*). No immunohistochemical signals were observed in the vessels of the arachnoid. Next, we investigated whether the CSF contains sAPP770β, the N-terminal β-secretase cleavage product of APP770. sAPP was pulled-down from CSF using heparin-agarose and then immunostained with anti-APP 22C11, anti-OX2 and anti-sAPPβ antibodies. We detected two bands with the anti-APP 22C11 antibody, of which only the upper band was detected with the anti-OX2 antibody (Fig. 5*D*), indicating that the upper band is derived from APP770. Since both the upper and lower bands were detected with the anti-sAPPβ antibody, both forms contain β-secretase cleavage products.

DISCUSSION

The dementia of AD is closely associated with accumulation of Aβ in the brain parenchyma and in the walls of blood vessels in the brain (25–27). Aβ deposition in the cerebral vasculature contributes to cerebral amyloid angiopathy, which shows a prevalence of >80% among AD individuals and 10–40% in elderly people without AD (28). Microbleeds in the brain occur in most cerebral amyloid angiopathy cases (25). Although important roles for cerebral vascular smooth muscle cells in vascular Aβ clearance were recently highlighted (29), the regions where vascular Aβ is produced for deposition remain to be determined.

We have shown for the first time that brain endothelial cells express APP770. First, we unambiguously detected APP770 expression in human BMECs. Using an anti-APP770 antibody that recognizes the OX2 domain for immunohistochemical staining of the cerebral cortex, we found that APP770 was expressed in venous and venular endothelial cells. We also showed that Aβ40 and Aβ42 were produced in BMECs. Therefore, our study points out the possibility that endothelial Aβ peptides could be the source of the Aβ deposits in cerebral vessel walls. Even though our immunohistochemical study is somewhat different from the previous observations in which Aβ deposits are frequently found in cortical arteries, the major distribution of APP770 in the brain might be different from where Aβ is mainly produced from APP770 to cause vascular Aβ deposits.

Perdivara *et al.* (16) recently identified the core 1 type *O*-glycans attached to residues Thr291, Thr292 and Thr576 of APP695. Here, we have shown that APP770 has an additional *O*-glycan chain at residue Thr353 within the OX2 domain. Furthermore, a series of site-directed mutations within the KPI domain had no effect on the mobility of APP770 (Fig. S3), indicating the absence of *O*-glycans in the KPI domain. A large ectodomain of APP consists of several subdomains, such as the E1 (30), E2 (31), and KPI domains (32). The web application POODLE-S (Prediction of Order and Disorder by Machine Learning) predicts that the other regions, in which all of the *O*-glycans are located, are intrinsically unstructured (33) (supplemental Fig. S4). Therefore, it is unlikely that the addition of any *O*-glycans to APP770 would result in conformational changes that might affect the α- or β-secretase cleavage. Because we found that *O*-glycosylated APP is selectively internalized, how *O*-glycosylation of APP would modulate its intracellular trafficking to the same intracellular compartment as α- and β-secretase remains an interesting and unanswered question. Because APP695 was also shown to contain *O*-glycans, whether our finding applies to neuronal APP also remains to be resolved. We found that BMECs expressed higher amounts of *O*-glycosylated APP770 than did COS cells, suggesting that endothelial cells possess a highly developed *O*-glycosylation machinery. Interestingly, endothelial *O*-glycan deficiency causes blood/lymphatic misconnections (34), indicating a fundamental role for *O*-glycans in vascular development.

In this study, we were able to discriminate CSF sAPP770β from other types of sAPPβ. As BACE1 seems to be a stress-response protein (35), one of our ongoing projects is elucidation of the critical factors required to increase sAPP770β secretion. We are now establishing a sandwich ELISA system to quantify sAPP770β in CSF or plasma. Because the CSF sAPP770β appears to be mainly derived from brain endothelial cells, sAPP770β would be a potential biomarker for diagnosing cerebrovascular dementia or AD.

Acknowledgments—We thank Dr. Shoichi Ishiura (The University of Tokyo) for the human APP751 and APP770 pcDNAs and Dr. Kei Maruyama (Saitama Medical School) for the anti-APP C15 antibody. We also thank Dr. Makoto Higuchi (National Institute of Radiological Sciences) for valuable discussions.

REFERENCES

1. Selkoe, D. J. (2001) *Physiol. Rev.* **81,** 741–766
2. Tanzi, R. E., and Bertram, L. (2005) *Cell* **120,** 545–555
3. Yan, R., Bienkowski, M. J., Shuck, M. E., Miao, H., Tory, M. C., Pauley, A. M., Brashier, J. R., Stratman, N. C., Mathews, W. R., Buhl, A. E., Carter, D. B., Tomasselli, A. G., Parodi, L. A., Heinrikson, R. L., and Gurney, M. E. (1999) *Nature* **402,** 533–537
4. Vassar, R., Bennett, B. D., Babu-Khan, S., Kahn, S., Mendiaz, E. A., Denis, P., Teplow, D. B., Ross, S., Amarante, P., Loeloff, R., Luo, Y., Fisher, S., Fuller, J., Edenson, S., Lile, J., Jarosinski, M. A., Biere, A. L., Curran, E., Burgess, T., Louis, J. C., Collins, F., Treanor, J., Rogers, G., and Citron, M. (1999) *Science* **286,** 735–741
5. Sinha, S., Anderson, J. P., Barbour, R., Basi, G. S., Caccavello, R., Davis, D., Doan, M., Dovey, H. F., Frigon, N., Hong, J., Jacobson-Croak, K., Jewett, N., Keim, P., Knops, J., Lieberburg, I., Power, M., Tan, H., Tatsuno, G., Tung, J., Schenk, D., Seubert, P., Suomensaari, S. M., Wang, S., Walker, D., Zhao, J., McConlogue, L., and John, V. (1999) *Nature* **402,** 537–540
6. Wolfe, M. S., Xia, W., Ostaszewski, B. L., Diehl, T. S., Kimberly, W. T., and Selkoe, D. J. (1999) *Nature* **398,** 513–517
7. De Strooper, B., Annaert, W., Cupers, P., Saftig, P., Craessaerts, K., Mumm, J. S., Schroeter, E. H., Schrijvers, V., Wolfe, M. S., Ray, W. J., Goate, A., and Kopan, R. (1999) *Nature* **398,** 518–522
8. Beher, D., Hesse, L., Masters, C. L., and Multhaup, G. (1996) *J. Biol. Chem.* **271,** 1613–1620
9. Small, D. H., Nurcombe, V., Moir, R., Michaelson, S., Monard, D., Beyreuther, K., and Masters, C. L. (1992) *J Neurosci.* **12,** 4143–4150
10. Reinhard, C., Hébert, S. S., and De Strooper, B. (2005) *EMBO J.* **24,** 3996–4006
11. Herms, J., Anliker, B., Heber, S., Ring, S., Fuhrmann, M., Kretzschmar, H., Sisodia, S., and Müller, U. (2004) *EMBO J.* **23,** 4106–4115
12. Ponte, P., Gonzalez-DeWhitt, P., Schilling, J., Miller, J., Hsu, D., Greenberg, B., Davis, K., Wallace, W., Lieberburg, I., and Fuller, F. (1988) *Nature* **331,** 525–527
13. Tanzi, R. E., McClatchey, A. I., Lamperti, E. D., Villa-Komaroff, L., Gusella, J. F., and Neve, R. L. (1988) *Nature* **331,** 528–530
14. Wertkin, A. M., Turner, R. S., Pleasure, S. J., Golde, T. E., Younkin, S. G., Trojanowski, J. Q., and Lee, V. M. (1993) *Proc. Natl. Acad. Sci. U.S.A.* **90,** 9513–9517
15. Xu, F., Davis, J., Miao, J., Previti, M. L., Romanov, G., Ziegler, K., and Van Nostrand, W. E. (2005) *Proc. Natl. Acad. Sci. U.S.A.* **102,** 18135–18140
16. Perdivara, I., Petrovich, R., Allinquant, B., Deterding, L. J., Tomer, K. B., and Przybylski, M. (2009) *J. Proteome Res.* **8,** 631–642
17. Kitazume, S., Imamaki, R., Ogawa, K., Komi, Y., Futakawa, S., Kojima, S., Hashimoto, Y., Marth, J. D., Paulson, J. C., and Taniguchi, N. (2010) *J. Biol. Chem.* **285,** 6515–6521
18. Hama, E., Shirotani, K., Masumoto, H., Sekine-Aizawa, Y., Aizawa, H., and Saido, T. C. (2001) *J. Biochem.* **130,** 721–726
19. Aroeti, B., and Mostov, K. E. (1994) *EMBO J.* **13,** 2297–2304
20. Koo, E. H., Sisodia, S. S., Archer, D. R., Martin, L. J., Weidemann, A., Beyreuther, K., Fischer, P., Masters, C. L., and Price, D. L. (1990) *Proc. Natl. Acad. Sci. U.S.A.* **87,** 1561–1565
21. Palmert, M. R., Podlisny, M. B., Witker, D. S., Oltersdorf, T., Younkin, L. H., Selkoe, D. J., and Younkin, S. G. (1989) *Proc. Natl. Acad. Sci. U.S.A.* **86,** 6338–6342
22. Sato, Y., Liu, C., Wojczyk, B. S., Kobata, A., Spitalnik, S. L., and Endo, T. (1999) *Biochim Biophys Acta.* **1472,** 344–358
23. Tomita, S., Kirino, Y., and Suzuki, T. (1998) *J. Biol. Chem.* **273,** 6277–6284
24. Ehehalt, R., Keller, P., Haass, C., Thiele, C., and Simons, K. (2003) *J. Cell. Biol.* **160,** 113–123
25. Vonsattel, J. P., Myers, R. H., Hedley-Whyte, E. T., Ropper, A. H., Bird, E. D., and Richardson, E. P., Jr. (1991) *Ann. Neurol.* **30,** 637–649
26. Van Broeckhoven, C., Haan, J., Bakker, E., Hardy, J. A., Van Hul, W., Wehnert, A., Vegter-Van der Vlis, M., and Roos, R. A. (1990) *Science* **248,** 1120–1122
27. Rovelet-Lecrux, A., Hannequin, D., Raux, G., Le Meur, N., Laquerrière, A., Vital, A., Dumanchin, C., Feuillette, S., Brice, A., Vercelletto, M., Dubas, F., Frebourg, T., and Campion, D. (2006) *Nat. Genet.* **38,** 24–26
28. Greenberg, S. M., Gurol, M. E., Rosand, J., and Smith, E. E. (2004) *Stroke* **35,** 2616–2619
29. Bell, R. D., Deane, R., Chow, N., Long, X., Sagare, A., Singh, I., Streb, J. W., Guo, H., Rubio, A., Van Nostrand, W., Miano, J. M., and Zlokovic, B. V. (2009) *Nat. Cell. Biol.* **11,** 143–153
30. Dahms, S. O., Hoefgen, S., Roeser, D., Schlott, B., Gührs, K. H., and Than, M. E. (2010) *Proc. Natl. Acad. Sci. U.S.A.* **107,** 5381–5386
31. Wang, Y., and Ha, Y. (2004) *Mol. Cell.* **15,** 343–353
32. Hynes, T. R., Randal, M., Kennedy, L. A., Eigenbrot, C., and Kossiakoff, A. A. (1990) *Biochemistry* **29,** 10018–10022
33. Shimizu, K., Hirose, S., and Noguchi, T. (2007) *Bioinformatics* **23,** 2337–2338
34. Fu, J., Gerhardt, H., McDaniel, J. M., Xia, B., Liu, X., Ivanciu, L., Ny, A., Hermans, K., Silasi-Mansat, R., McGee, S., Nye, E., Ju, T., Ramirez, M. I., Carmeliet, P., Cummings, R. D., Lupu, F., and Xia, L. (2008) *J. Clin. Invest.* **118,** 3725–3737
35. Vassar, R., Kovacs, D. M., Yan, R., and Wong, P. C. (2009) *J. Neurosci.* **29,** 12787–12794

Journal of the Neurological Sciences 299 (2010) 155–162

Contents lists available at ScienceDirect

Journal of the Neurological Sciences

journal homepage: www.elsevier.com/locate/jns

Capillary CAA and perivascular Aβ-deposition: Two distinct features of Alzheimer's disease pathology

Johannes Attems [a], Haruyasu Yamaguchi [b], Takaomi C. Saido [c], Dietmar Rudolf Thal [d,*]

[a] Institute for Ageing and Health, Newcastle University, Newcastle upon Tyne, UK
[b] Gunma University School of Health Sciences, Maebashi, Gunma 371-8514, Japan
[c] Laboratory of Proteolytic Neuroscience, RIKEN Brain Science Institute, 351-0198 Saitama, Japan
[d] Institute of Pathology, Laboratory of Neuropathology, University of Ulm, D-89081 Ulm, Germany

ARTICLE INFO

Article history:
Received 24 March 2010
Received in revised form 23 June 2010
Accepted 22 August 2010
Available online 17 September 2010

Keywords:
Cerebral amyloid angiopathy
Alzheimer's disease
Capillaries
Amyloid β-protein
Apolipoprotein E
Pericapillary amyloid

ABSTRACT

Cerebral amyloid angiopathy (CAA) is frequently seen in Alzheimer's disease (AD) cases and represents one of its histopathological hallmarks. CAA is characterized by amyloid β-protein (Aβ) deposits within vessel walls. In addition to arteries and veins capillaries can also be affected. Aβ deposition into the capillary wall is, thereby, known as capillary CAA (capCAA) and strongly associated with the apolipoprotein E *APOE*ε4 allele as a risk factor. Aβ deposits along the pericapillary glia limitans are described as pericapillary Aβ (pericapAβ: synonymous with pericapillary CAA in other studies). Here, we studied the relationship between pericapAβ and capCAA in 58 human autopsy cases. Although pericapAβ and capCAA were more frequently found in AD cases compared to controls and although they exhibited a correlation to one another, detailed analysis revealed that there is a significant number of cases with pericapAβ lacking capCAA and vice versa. Moreover, single capillaries show either both pathologies or pericapAβ or capCAA only. There was no local association between these pathologies when analyzing multiple capillaries in each given case. Moreover, pericapAβ predominantly exhibited $Aβ_{42}$ whereas capCAA contained both $Aβ_{42}$ and $Aβ_{40}$. These differences as well as differences in the related astroglial reaction indicate that pericapAβ and capCAA are not directly linked. PericapAβ appears to represent initial Aβ accumulation along the glia limitans that is involved in the perivascular drainage of apoE and Aβ regardless of the *APOE* genotype whereas capCAA could be explained by a limited transendothelial clearance of apoE4–Aβ complexes compared to apoE2/3–Aβ complexes.

1. Introduction

Alzheimer's disease (AD) is histopathologically characterized by the deposition of the amyloid β-protein (Aβ) and by the generation of neurofibrillary tangles (NFTs) [1,2]. In addition to parenchymal Aβ-plaques Aβ is also deposited in the vessel wall referred to as cerebral amyloid angiopathy (CAA) [3–6]. Vascular Aβ-deposition has also been demonstrated in transgenic mice that express APP driven by a neuron-specific promoter indicating that neuron-derived Aβ is the subject of deposition in the vessel wall [7]. Drainage along perivascular channels and basement membranes was identified as an important clearance mechanism for neuron-derived Aβ [8,9]. Alterations of the perivascular clearance of Aβ are related to vessel wall changes due to small vessel disease [9,10] resulting in an alteration of the blood-brain barrier (BBB) at least in the precapillary segment [11,12].

Apolipoprotein E (apoE) is involved in physiological perivascular clearance of the extracellular fluid [13] and its *APOE* ε4 allele has been reported to be a major risk factor for sporadic AD [14,15]. Moreover, Aβ-deposition in the walls of capillaries (capCAA) is strongly associated with the *APOE* ε4 allele constituting the distinction of two types of CAA: CAA-type 1 representing capCAA with or without CAA in arteries and/ or veins whereas CAA-type 2 refers to CAA cases without capCAA [16]. By contrast, parenchymal Aβ-deposits clustered along the glia limitans around capillary walls are predominately composed of $Aβ_{42}$ and increase in frequency with the progression of AD [17,18] whereas capCAA is detected in only 51% of AD cases [19]. Due to the anatomical relationship of these pericapillary Aβ-deposits they were also named capCAA previously [17] but here will be referred to as pericapillary Aβ deposits (pericapAβ). PericapAβ represents parenchymal Aβ-deposits around capillaries regardless whether the capillaries contain Aβ-deposits within their wall [17]. This pericapAβ is different from the dyshoric plaques that are, by definition attached to capillary Aβ-deposits [16,20]. It is not clear whether capCAA and pericapAβ are biologically linked or whether they represent two different features of AD pathology. However, capillaries as well as astrocytes

* Corresponding author. Institute of Pathology, Laboratory of Neuropathology, University of Ulm, Helmholtzstrasse 8/1, D-89081 Ulm, Germany. Tel.: +49 8221 96 2163; fax: +49 8221 96 28158.
E-mail address: Dietmar.Thal@uni-ulm.de (D.R. Thal).

0022-510X/$ – see front matter © 2010 Elsevier B.V. All rights reserved.
doi:10.1016/j.jns.2010.08.030

constituting the glia limitans represent important parts of the BBB. It is, therefore, tempting to assume a link between both, capCAA and pericapAβ, and alterations of the BBB integrity including glia limitans function.

To address these questions we studied 58 human autopsy cases with and without capCAA and pericapAβ. Our results show that capCAA and pericapAβ are not directly linked but that both pathologies point to alterations in Aβ-clearance from brain.

2. Materials and methods

2.1. Neuropathology and human sample characterization

Our cohort consists of 58 non-selected autopsy cases from the Pathological Institute of the Otto Wagner Hospital (Vienna, Austria) and the Municipal hospital of Offenbach am Main (Germany). All autopsies and tissue retrieval were performed in accordance to the Austrian and German laws. This study was approved by the local ethical committee. The patient age ranged between 62 and 104 years (mean 84.7 years, ±8.45 years; 33 female, 25 male). This sample included 23 AD cases and 35 non-AD controls (Table 1). Non-AD controls included non-demented cases with and without Aβ-deposition and NFTs, cases with argyrophilic grain disease, vascular lesions, Parkinson's disease and NFT-predominant dementia (Table 1). Demented as well as non-demented patients had been examined 1–4 weeks prior to death according to standardized protocols utilized for routine clinical and neurological examinations of patients upon admission to hospital. These protocols included the assessment of cognitive function and the ability to perform activities associated with daily life: care for and dress oneself, eating habits, bladder and bowel continence, speech patterns, reading and writing skills, short-term and long-term memory, and orientation within the hospital setting. These data were used to determine whether individuals clinically fulfilled the DSM-IV criteria for dementia [21]. AD was diagnosed when dementia was observed and when the degree of AD-related pathology indicated a high likelihood for AD according to standardized criteria [22]. In the event that there were no further changes in a demented brain than AD pathology with an intermediate likelihood for the disease these cases were also classified as AD. The likelihood for AD was assessed strictly following the recommended criteria [22]. A given likelihood was diagnosed only in the event that both CERAD and Braak NFT-stage met the criteria with the exception that cases with Braak NFT-stages V and VI and sparse neuritic plaques (i.e. CERAD-score 1) were supposed to have an intermediate likelihood for AD.

The brains were fixed in a 4% aqueous formaldehyde solution for at least three weeks and underwent neuropathological screening. Blocks from the medial temporal lobe (MTL) were excised at the levels of the anterior limit of the dentate gyrus, and/or the level of the lateral geniculate body [23] as well as from the occipital cortex (Brodmann areas 17, 18, and 19). All tissue blocks were embedded in paraffin. The paraffin blocks were sectioned at 10 μm.

Neurofibrillary changes were detected using the Gallyas silver-staining method as well as anti-τ-immunohistochemistry (AT8, Innogenetics, Belgium, 1/1000) [24–27]. Neuritic plaques were diagnosed either in Gallyas- or Bielschowsky-stained sections. The presence of amyloid deposits was assessed using anti-Aβ immunohistochemistry (4G8, Covance, Emeryville, CA, USA [28], 1/5000, formic acid pretreatment).

Diagnosis of the stages in the development of neurofibrillary changes (Braak NFT-stage) and the semiquantitative assessment of neuritic plaques (CERAD-score) were performed in accordance with published and recommended criteria [22,26,29,30]. For staging of Aβ-pathology, we used a previously published protocol for four phases of β-amyloidosis in the MTL [31]. This hierarchically-based procedure facilitates study of the topographic distribution pattern of Aβ-deposition in additional brain regions [31,32]: *Phase 1* represents Aβ-deposition that is restricted to the temporal neocortex. *Phase 2* is characterized by the presence of additional Aβ-plaques in the entorhinal cortex and/or in the subiculum-CA1 region. *Phase 3* is marked by the presence of Aβ-plaques in the outer zone of the molecular layer of the fascia dentata, subpial band-like amyloid, and/or presubicular "lake-like" amyloid. The existence of further Aβ-plaques in CA4 and/or the pre-α layer of the entorhinal cortex characterizes *phase 4* of Aβ-deposition in the MTL.

CAA was diagnosed whenever vascular Aβ-deposition was observed and the severity of CAA was graded according to Vonsattel [33]. For subclassification of CAA types, we noted whether capillary Aβ-deposits were present. In the event of capillary Aβ-deposition, cases were classified as CAA-type 1 (capCAA), whereas those lacking capillary Aβ but having Aβ-deposits in arteries or veins were referred to as CAA-type 2 [16]. In addition, we assessed the extent of pericapAβ that was defined by linear Aβ-deposits along the glia limitans frequently associated with adjacent Aβ-deposits in the surrounding neuropil. The glia limitans constitutes the border between the perivascular space (i.e. Virchow–Robin space) and the brain parenchyma [34], and is, thus, easily identified by its morphology.

2.2. Immunohistochemistry

In each case, abnormal phosphorylated τ-protein was visualized with a monoclonal antibody (AT-8) and Aβ in plaques, vessels and pericapillary deposits using an antibody raised against $Aβ_{17-24}$ (4G8). In five representative cases, ApoE was detected using a monoclonal antibody (Covance: D6E10 [13], 1/500, 24 h at 22 °C, microwave and formic acid pretreatment). The primary antibodies were detected either with a biotinylated secondary antibody and the ABC complex (Vectastain: Vector Laboratories, Burlingame, CA, USA), and this reaction was subsequently visualized with 3,3-diaminobencidine (DAB) or with an alkaline phosphatase labeled secondary antibody visualized with Permanent Red® (Dako, Glostrup, Denmark). Immunostained paraffin sections were counterstained with hematoxylin. Positive and negative controls were included.

Double immunolabeling was performed to demonstrate the spatial relationship between apoE, glial fibrillary acidic protein (GFAP) expression, and vascular Aβ-deposition. GFAP was visualized either with a polyclonal rabbit IgG antibody (1/1000, DAKO, 24 h at 22 °C) or with a monoclonal antibody (1/20, G-A-5, Boehringer-Mannheim, 24 h at 22 °C), and Aβ either with anti-$Aβ_{17-24}$ (4G8), anti-$Aβ_{42}$ (1/200, MBC42, 24 h at 22 °C [35]) or with a polyclonal antibody directed against $Aβ_{N1D}$ (1/100, [36], 24 h at 22 °C, microwave and formic acid pretreatment). Antibodies directed against the N-terminus of Aβ have been shown to stain all vascular Aβ-deposits just as C-terminus specific anti-Aβ-antibodies [16,37]. One primary antibody was detected with a carbocyanine 2-labeled secondary antibody specifically directed against either mouse or rabbit IgG (Dianova, Hamburg, Germany), whereas the second primary antibody was detected using a carbocyanine 3-labeled secondary antibody specifically directed against either mouse or rabbit IgG (Dianova, Hamburg, Germany). All tissue sections were viewed with a Leica DMLB fluorescence microscope. Digital photographs were obtained with a Leica DC 500 camera and were edited for publication layout with the assistance of a CorelPhotopaint® software, release 12.0.

2.3. Morphological analysis

To clarify whether capCAA and pericapAβ depend on one another we assessed whether the cases exhibited capCAA and/or pericapAβ.

To determine the local relationship between pericapAβ and capCAA we restricted our analysis to the 27 cases with capCAA.

Table 1
List of cases.

Case nr.	Gender	Age (years)	CAA-type	Severity of CAA	Pericapillary Aβ	Aβ-phase	CERAD	Braak NFT-stage	NIA-Reagan	Diagnosis
1	f	80	0	0	No	0	0	1	Low	Age associated
2	m	71	0	0	No	1	0	1	Low	Age associated
3	m	70	1	1	No	1	0	1	Low	Age associated
4	f	84	1	1	Yes	1	0	1	Low	AGD
5	m	80	2	3	No	1	0	1	Low	Hemorrhage
6	f	87	0	0	Yes	2	0	1	Low	Age associated
7	m	82	0	0	Yes	2	0	1	Low	PD
8	f	98	0	0	Yes	2	0	1	Low	Mixed (VD-AGD)
9	f	91	2	1	Yes	2	1	1	Low	Age associated
10	f	81	1	2	Yes	3	1	1	Low	Age associated
11	m	90	2	2	Yes	4	2	1	Low	Hippocampal sclerosis
12	f	89	0	0	No	0	0	2	Low	Deep hemorrhage
13	m	94	0	0	No	0	0	2	Low	Infarct
14	f	80	0	0	No	0	0	2	Low	AGD
15	f	89	0	0	No	0	0	2	Low	AGD
16	m	77	0	0	No	1	0	2	Low	AGD
17	m	86	1	2	No	1	0	2	Low	AGD
18	m	82	2	1	No	1	0	2	Low	Age associated
19	m	83	1	2	Yes	2	1	2	Low	VD
20	m	76	0	0	Yes	3	1	2	Low	AGD
21	m	92	1	1	Yes	3	0	2	Low	AGD
22	f	62	1	2	Yes	4	1	2	Low	AGD
23	f	98	0	0	No	0	0	3	Low	PD
24	m	84	0	0	No	0	0	3	Low	Age associated
25	f	94	1	1	No	1	0	3	Low	Deep hemorrhage
26	f	90	2	1	No	1	0	3	Low	NFD
27	m	77	0	0	Yes	2	1	3	Low	VD
28	f	104	1	2	Yes	2	0	3	Low	Age associated
29	f	101	2	1	Yes	2	3	3	Intermediate	AD
30	f	85	0	0	No	3	1	3	Low	AD
31	m	91	1	2	Yes	3	1	3	Low	VD
32	m	87	1	2	Yes	3	1	3	Low	Age associated
33	m	82	1	2	Yes	3	2	3	Intermediate	AD
34	f	96	2	1	Yes	3	2	3	Intermediate	AGD
35	f	63	0	0	Yes	4	1	3	Low	Hemorrhage
36	f	85	0	0	Yes	4	2	3	Intermediate	Age associated
37	f	79	2	1	Yes	4	1	3	Low	Age associated
38	m	81	2	1	Yes	4	1	3	Low	AGD
39	f	92	1	1	Yes	3	3	4	Intermediate	AD
40	m	85	1	2	Yes	4	2	4	Intermediate	AD
41	m	70	1	1	Yes	4	3	4	Intermediate	AD, PD
42	f	92	1	2	Yes	4	3	4	Intermediate	AD
43	f	79	2	1	Yes	4	3	4	Intermediate	AD
44	m	90	2	1	Yes	4	3	4	Intermediate	AD
45	f	90	2	2	Yes	3	2	5	Intermediate	AD
46	f	88	2	3	Yes	3	3	5	High	AD
47	m	89	2	1	Yes	3	3	5	High	AD
48	m	72	1	2	Yes	4	2	5	Intermediate	AD
49	f	95	1	2	Yes	4	2	5	Intermediate	AD
50	m	75	1	1	Yes	4	3	5	High	AD
51	f	80	1	3	Yes	4	3	5	High	AD, PD
52	f	94	1	2	Yes	4	2	5	Intermediate	AD
53	f	84	1	2	Yes	4	3	5	High	AD
54	f	85	1	3	Yes	4	3	5	High	AD
55	f	81	1	1	Yes	4	1	5	Intermediate	AD
56	m	74	1	1	Yes	3	3	6	High	AD
57	f	84	1	1	Yes	3	2	6	Intermediate	AD
58	f	77	1	3	Yes	3	3	6	High	AD

Abbreviations: CAA, cerebral amyloid angiopathy; Aβ, amyloid β-protein; CERAD, Consortium to Establish a Registry for Alzheimer's Disease (AD) are semiquantitative neuropathological diagnostic criteria based on the density of neocortical neuritic plaques as reported by Mirra et al. [30]: 0 = no neuritic plaques, 1 = neuritic plaques: sparse, 2 = neuritic plaques: moderate, 3 = neuritic plaques: frequent; Braak NFT-stage, Braak neurofibrillary tangle stage represents the extension of neurofibrillary tangles throughout the brain according to Braak and Braak [29]; NIA-Reagan, the National Institute on Aging and Reagan Institute Working Group Criteria are neuropathological criteria that state the likelihood of clinical dementia caused by AD [22]; m, male; f, female; AD, Alzheimer's disease; age associated, no other pathology beyond age associated changes; AGD, agyrophilic grain disease; PD, Parkinson's disease; VD, vascular dementia; mixed, mixed dementia; NFD, neurofibrillary tangle predominant dementia.

Here, we studied the entorhinal cortex, the CA1-subiculum subfield, and the occipital cortex (Brodmann areas 17, 18, and 19) in this order. First, we observed ten consecutive vessel profiles affected by capCAA for its association with pericapAβ. Second, we examined ten consecutive capillary profiles within pericapAβ for its co-occurrence of capCAA. In the event that there were less than ten capillary profiles for a given pathology all affected capillary profiles were examined. All kinds of capillary profiles were subsequently assessed to avoid investigator driven bias. The analysis of longitudinal and cross sectioned profiles of capillaries is aimed at analyzing the direct local relation between capCAA and pericapAβ on a stochastic basis but does not allow conclusions about the absence of capCAA or pericapAβ in the entire capillary intersections. These data were used to calculate the percentages of capCAA-affected capillary profiles with pericapAβ and the percentage of capillary profiles with pericapAβ associated with capCAA.

Table 2
Occurrence of pericapAβ-deposition and capCAA. Only 3 cases exhibited capCAA in the absence of pericapAβ whereas pericapAβ was seen in 18 cases lacking capCAA.

	No capillary CAA	Capillary CAA
No pericapillary Aβ-deposits	13	3
Pericapillary Aβ-deposits	18	24

2.4. Statistical analysis

To clarify whether capCAA and pericapAβ are linked the Sign-test was used. Comparisons between AD and non-AD cases, capCAA and non-capCAA cases, and pericapAβ and non-pericapAβ cases were performed using the Mann–Whitney U-test. Correlations were calculated using partial correlation analysis controlled for age and gender. Computations were performed with the help of the PASW-Statistics® software, release 18.0.0.

3. Results

PericapAβ and capCAA either occurred in the same cases or pericapAβ was found in the complete absence of capCAA or vice versa (Tables 1 and 2). Among individual cases the occurrence of pericapAβ differed from that of capCAA (sign-test: $p<0.001$). In cases that exhibited both, capCAA and pericapAβ, most of them showed less than 50% local co-occurrence of capCAA and pericapAβ in vessel profiles with capCAA (Fig. 1A) as well as in capillaries with pericapAβ (Fig. 1B) although single cases exhibited 80–100% local co-occurrence (Fig. 1A and B).

Analyzing individual vessels histologically, we found capillaries showing the characteristic morphology of both capCAA and pericapAβ (Fig. 2A) but also pericapAβ lacking Aβ in the capillary wall (Fig. 2B) and capCAA without pericapAβ (Fig. 2C). In capCAA as well as in pericapAβ, Aβ deposits were found to contain apoE (Fig. 2D–F). Statistical analysis revealed that there was no significant correlation between the occurrence of capCAA in capillary profiles within pericapAβ and that of pericapAβ in capCAA-affected vessels (partial correlation analysis controlled for age and gender: $r=0.318$, $p=0.121$; Fig. 1C). The sign-test indicated significant differences in the association between capCAA and pericapAβ in capCAA cases with regard to the perspective of analysis ($p = 0.041$). In other words, analyzing capCAA-affected vessels for pericapAβ leads to different results compared to studying capillary profiles with pericapAβ for capCAA. For example, one case did not exhibit capCAA in the 10 consecutive capillary profiles observed for the local association between pericapAβ and capCAA (i.e. less than 10% of the capillary profiles with pericapAβ exhibit capCAA). However, the same case showed, when focusing only on the few vessels with capCAA, pericapAβ around 50% of the capCAA-affected capillary profiles. Conversely, other cases with capCAA and pericapAβ failed to show both pathologies in the same capillary profiles (Fig. 1C) indicating a high variability in the local co-occurrence of capCAA and pericapAβ among our cases.

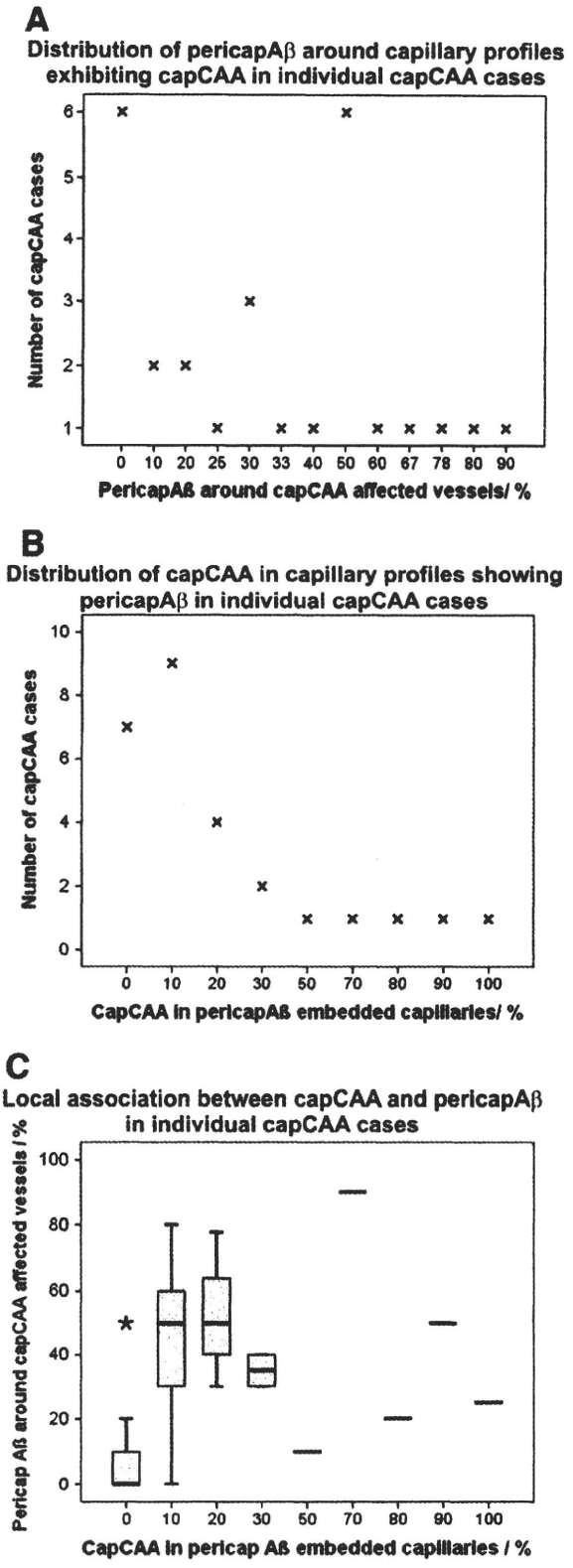

Fig. 1. A: The figure shows the number of capCAA cases, in which capCAA-affected vessels exhibited pericapAβ in a given percentage, e.g., in six cases capCAA-affected vessels were free of pericapAβ and in only one case there was 90% co-localization. B: This figure depicts the number of capCAA cases, in which capillary profiles with pericapAβ exhibited capCAA in a given percentage, e.g., in 7 cases capillary profiles with pericapAβ were free of capCAA whereas only one case showed 100% co-localization. C: The boxplot diagram demonstrates the variability in the local relationship between capCAA and pericapAβ. Some cases showed co-occurrence of both pathologies whereas other cases displayed both pathologies in separate parts of the capillaries without any co-localization. There was also one capCAA case, in which less than 10% of the capillary profiles with pericapAβ exhibited capCAA (depicted in the 0% category) but despite the high prevalence of pericapAβ 50% of all capCAA-affected vessels exhibited pericapAβ as well. The x-axis indicates how many percent of capillary profiles with pericapAβ also exhibit capCAA. The y-axis demonstrates how many percent of the CAA-affected capillaries also showed pericapAβ. There was no significant local relationship between capCAA and pericapAβ (partial correlation analysis: $r=0.318$, $p=0.121$).

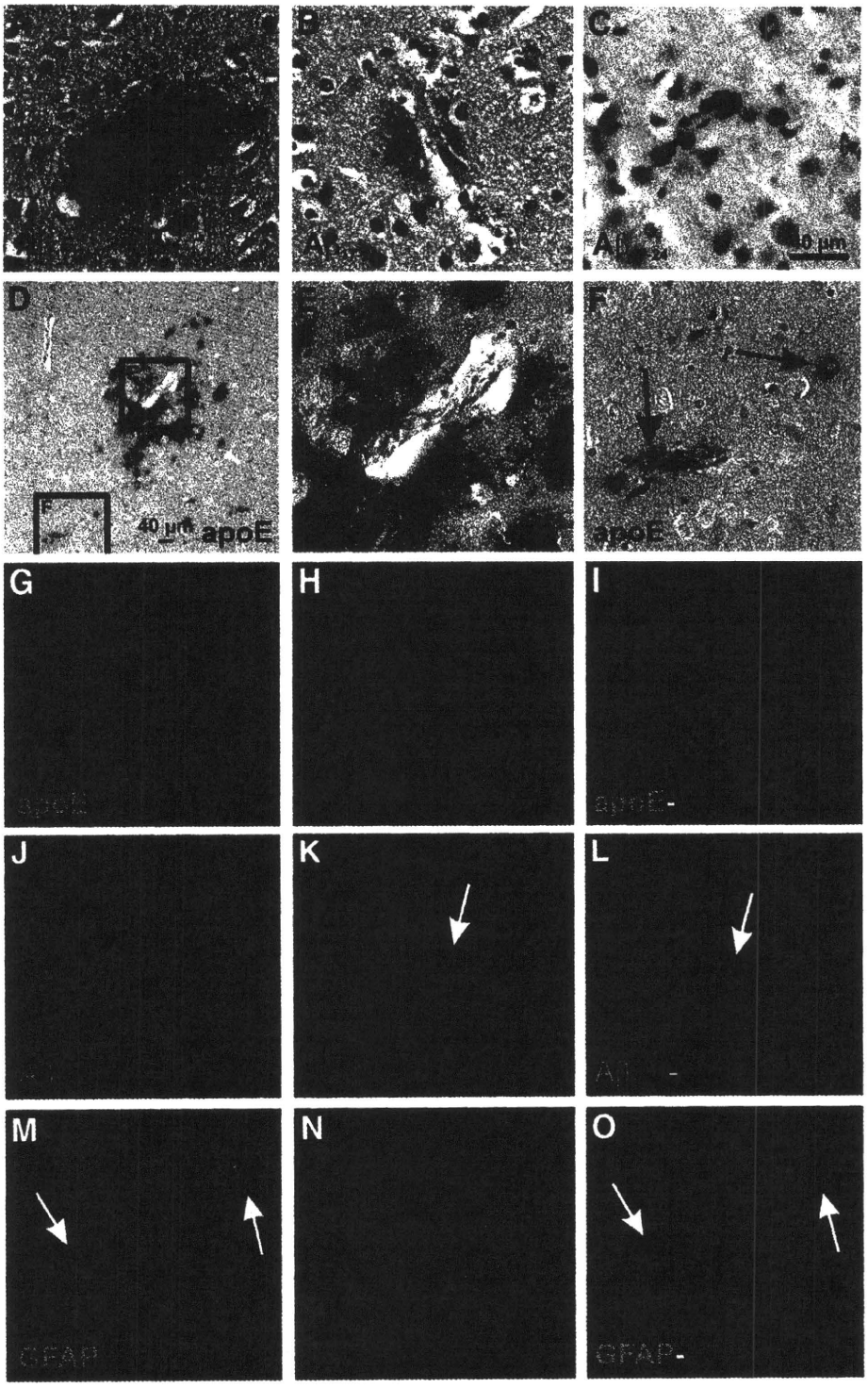

Fig. 2. A–C: CapCAA and pericapAβ can occur at the same capillary (A) or separately, i.e. pericapAβ without capCAA (B) or capillary CAA without pericapAβ (C). CapCAA, thereby, consists of Aβ-deposits attached to the basement membrane of the capillaries often showing the pattern of dyshoric angiopathy [20,61] (C). D–F: ApoE is also deposited in capCAA and pericapAβ even in the same case at different places (D). The boxes indicate the areas enlarged in E and F as depicted. Panel E displays an enlargement of the apoE-positive pericapAβ. Note that the central capillary does not exhibit apoE-positive Aβ-deposits within the vessel wall. Panel F shows capCAA-affected capillaries exhibiting apoE (arrows). Here, there is no association with pericapAβ. G–I: ApoE-positive pericapAβ (G) often does not exhibit Aβ-epitopes which are detectable with antibodies raised against N-terminal epitopes such as the $A\beta_{N1D}$-antibody (H, I). J–L: PericapAβ as detected with the anti-$A\beta_{17-24}$ antibody (J) is not associated with severe astrocytosis but exhibits a weak labeling of the astrocytic processes (arrow in K) that are associated with the pericapAβ (arrow in L). M–O: Severe astrogliosis exhibiting reactive astrocytes (arrows in M) was found in association with capCAA (N, arrows in O). Staining was performed as indicated and color-coded. Calibration bars in C and D corresponds to 40 µm. The calibration bar in C is valid for panels A–C and E–O.

Both capCAA and pericapAβ were found more frequently in AD cases than in non-AD cases (Mann–Whitney U-test: capCAA: $p=0.001$; pericapAβ: $p=0.002$), and they were correlated to one another (Partial correlation analysis: $r=0.354$, $p=0.007$) as well as with Braak NFT-stage, CERAD neuritic plaque score and the phase of Aβ-deposition (pericapAβ–NFT: $r=0.402$, $p=0.002$, CERAD: $r=0.564$, $p<0.001$, Aβ-phase: $r=0.809$, $p<0.001$; capCAA–NFT: $r=0.484$, $p<0.001$, CERAD: $r=0.473$, $p<0.001$, Aβ-phase: $r=0.525$, $p<0.001$).

Double label immunohistochemistry revealed that pericapAβ was detectable with antibodies against the C-terminus of Aβ or against C-terminal epitopes including $Aβ_{17-24}$ as well as with anti-apoE. However, N-terminal epitopes were less frequently observed in pericapAβ as demonstrated in a double label immunohistochemistry experiment (Fig. 2G–I). Reactive astrocytes were not observed in association with pericapAβ whereas a fine GFAP-positive network of astrocytic processes was seen in pericapAβ (Fig. 2J–L). CapCAA, on the other hand, induced a strong astroglial response as demonstrated by the GFAP-positive reactive astrocytes near Aβ-deposits in capillaries (Fig. 2M–O).

4. Discussion

Our results show that capCAA and pericapAβ represent two distinct capillary-associated Aβ pathologies of both AD patients and controls. Arguments in favor of this interpretation are that 1) pericapAβ and capCAA occur in different anatomical structures, i.e. pericapAβ along the glia limitans and capCAA at the basement membrane of the capillary wall, 2) pericapAβ occurs in cases lacking capCAA and vice versa, 3) pericapAβ frequently exhibited $Aβ_{42}$-deposits [18] lacking N-terminal epitopes whereas capCAA contains $Aβ_{40}$ and N-terminal epitopes of Aβ are detectable [16], and 4) capCAA was associated with reactive astrogliosis whereas pericapAβ was not. This suggests that there is no direct pathogenetic link between capCAA and pericapAβ.

Our analysis of double labeled sections revealed that apoE co-localizes both capCAA and pericapAβ. PericapAβ co-localizing apoE often did not exhibit N-terminal Aβ-epitopes indicating that pericapAβ often consists of so-called "N-terminal truncated" Aβ similar as cerebellar Aβ-deposits [38], fleecy amyloid [39], and early Aβ-plaques [40]. It is not clear whether these "N-terminal truncated" Aβ-deposits are really truncated or whether the N-terminus is just hidden, e.g. by apoE or by fixation as discussed earlier [41,42]. However, these Aβ-deposits have been identified to represent early deposits [40–42] and, therefore, it is tempting to speculate that pericapAβ represents an early form of Aβ-deposits. This hypothesis is supported by our finding that pericapAβ does not induce severe astrogliosis, which is often associated with amyloid plaques [43]. Moreover, the co-localization with fine astrocyte processes gives rise to the assumption that pericapAβ is similar to Aβ in perivascular astrocytes around larger vessels [10] and within the subpial band-like amyloid [44] and may represent a very early symptom of an altered vascular/ perivascular clearance of Aβ. This hypothesis is further supported by our previous findings of "vanishing" diffuse plaques in the occipital cortex that seem to be absorbed by astrocytes [35] and of fleecy amyloid in the entorhinal cortex that is absorbed by astrocytes leaving behind diffuse and cored plaques [45]. Both "vanishing" diffuse plaques and fleecy amyloid are also found in the glia limitans and, hence, fulfill the criteria of pericapAβ. The absorption of Aβ by astrocytes and their presumable contribution to perivascular clearance in association with apoE [13] suggest that pericapAβ represents initial imbalances in apoE-associated astroglial Aβ uptake and perivascular drainage. This hypothesis is supported by the finding of pericapAβ in amyloid precursor protein (APP) transgenic mice expressing APP in neurons indicating that pericapAβ is neuron derived [46] and presumably subject to vascular/perivascular clearance.

CapCAA, on the other hand, is associated with severe reactive astrocytosis and contains Aβ that exhibits $Aβ_{42}$, $Aβ_{40}$ [16], N-terminal epitopes of Aβ such $Aβ_{N1D}$, and apoE. Hence, capCAA is likely to be the result of a severely impaired vascular/perivascular Aβ drainage. Since capCAA is mainly restricted to *APOE* ε4-carriers [16,47,48] it is tempting to speculate that apoE4 impairs the vascular/perivascular clearance of Aβ in a way that Aβ already aggregates in the capillary wall and induces severe astrocytosis. Possible explanations for such an *APOE* ε4-specific pathology are 1) the low endothelial transcytosis efficiency for apoE4-Aβ complexes whereas apoE2-Aβ and apoE3-Aβ complexes are readily cleared by transcytosis [49] and 2) the reduced production of apoE by perivascular cells in *APOE* ε4 allele carriers [50]. Therefore, apoE4–Aβ complexes and Aβ accumulate at the basement membrane of *APOE* ε4 carriers leading to capCAA (Fig. 3). An argument against the hypothesis that capCAA represents the morphological hallmark of a distinct type of CAA or AD is that *APOE*

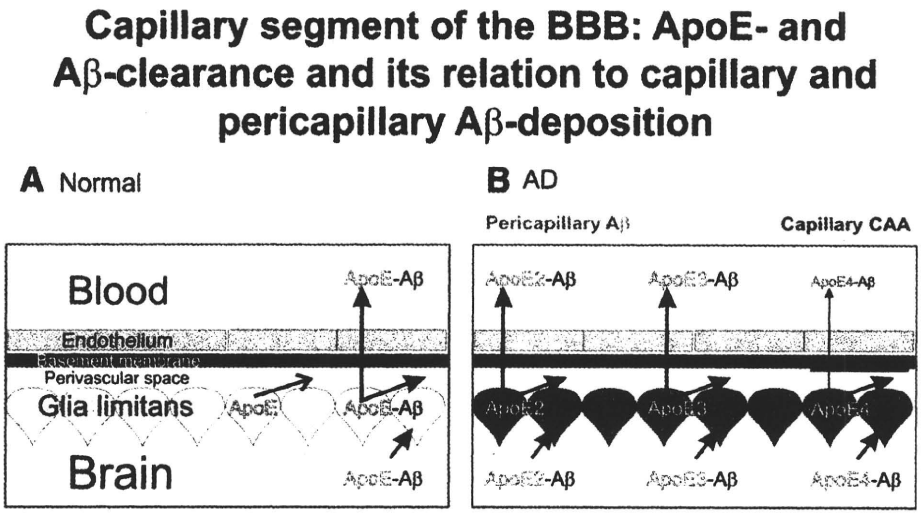

Fig. 3. Schematic representation of the clearance of apoE and apoE–Aβ complexes at the capillary segment of the Blood-brain barrier (BBB). A: Under normal conditions apoE and apoE–Aβ complexes are cleared through the glia limitans into the perivascular space, along the basement membranes into the cervical lymph nodes [8], and via transcytosis through endothelial cells into the blood [49]. B: In AD Aβ generally accumulates at the glia limitans and apoE4–Aβ complexes are less efficiently cleared via endothelial transcytosis than apoE2-Aβ and apoE3–Aβ complexes [49] resulting in capCAA in *APOE* ε4 carriers. The decreased production of apoE by pericytes of *APOE* ε4 carriers [50] may also contribute to a reduced perivascular clearance of Aβ in *APOE* ε4 carriers and its subsequent accumulation at the vessel wall.

ε4 is merely a risk factor for CAA in general and the association between capCAA and the *APOE* ε4 allele is explained by the assumption that capCAA represents the end stage of CAA [51]. However, in our previous work we have shown that capCAA was observed in non-demented cases with Aβ-phase 1, i.e. the initial stage of Aβ-deposition [16]. Thus, capCAA is not restricted to end-stage CAA or end-stage AD but identifies a distinct type of CAA and AD pathology strongly associated with the *APOE* ε4 allele [16,47].

It has been discussed that blood- and vessel wall-derived proteins may contribute to the development of CAA and pericapAβ-deposition [52–54]. The "dyshoric" pattern of capCAA with deposits attached to the basement membrane entering the parenchyma [20] as well as the detection of siderin and blood-derived proteins in Aβ-deposits [52,55–57] may support this hypothesis. However, the development of CAA in mice with transgenic Aβ production limited to neurons strongly suggests that Aβ in CAA represents accumulated neuron-derived Aβ that has been cleared from the brain. Moreover, vessel wall alterations due to CAA may result in a BBB-leakage and explain the influx of plasma proteins and blood into the brain parenchyma [58,59]. Thus, a contribution of blood- and vessel wall-derived proteins leaking into the brain through CAA- and small vessel disease-affected vessels [10] does not argue against the assumption that Aβ is cleared from the brain by astrocytes [35,45,60] and secreted into the perivascular space for clearance. ApoE plays an important role in this process [10,13] that is influenced by the *APOE* genotype.

Whether capCAA leads to an alteration of the BBB is not clear because 1) reactive astrocytes near capCAA could be a reaction to the Aβ deposition, 2) capCAA frequently lacks pericapAβ, which would be expected to occur in the event of plasma leakage into brain, and 3) a leakage of plasma proteins has been observed already at the precapillary level of the BBB [10,12] explaining the well-known occurrence of plasma proteins in the brain parenchyma of AD patients [55,56].

In conclusion, our results indicate that pericapAβ represents an early form of Aβ-deposits presumably pointing to an alteration of the apoE-related clearance of Aβ through the glia limitans into the perivascular space and along the vascular basement membrane [8] whereas capCAA represents a distinct pathology genetically associated with the *APOE* ε4 allele [16,47] and related to a decreased transcytosis of apoE4–Aβ complexes through the endothelium into the blood [49] (Fig. 3). There is no direct link between pericapAβ and capCAA, indicating that alterations of the perivascular clearance of Aβ appear to contribute to the development of AD-related Aβ-deposition regardless of the histopathological subtype of CAA or AD.

Disclosure statements

This study was supported by DFG grants TH624/4-1 and TH624/4-2 (DRT) and the Newcastle NIHR Biomedical Research Centre in Ageing and Age Related Diseases (JA). The funding bodies had no influence on study design, conduction, interpretation and submission of the results.

Acknowledgments

The authors thank Irina Lungrin and Katrin Pruy for their technical help. The authors thank Dr. Peter Müller and Dr. Mario Orantes (Offenbach am Main, Germany) for providing autopsy tissue.

References

[1] Alzheimer A. Ueber eine eigenartige Erkrankung der Hirnrinde. Allg Zschr Psych 1907;64:146–8.
[2] Masters CL, Simms G, Weinman NA, Multhaup G, McDonald BL, Beyreuther K. Amyloid plaque core protein in Alzheimer disease and Down syndrome. Proc Natl Acad Sci USA 1985;82:4245–9.
[3] Joachim CL, Morris JH, Selkoe DJ. Clinically diagnosed Alzheimer's disease: autopsy results in 150 cases. Ann Neurol 1988;24:50–6.
[4] Scholz W. Studien zur Pathologie der Hirngefäße. II. Die drusige Entartung der Hirnarterien und -capillaren. (Eine Form seniler Gefäßerkrankung). Z ges Neurol Psychiatr 1938;4:694-715
[5] Revesz T, Holton JL, Lashley T, et al. Genetics and molecular pathogenesis of sporadic and hereditary cerebral amyloid angiopathies. Acta Neuropathol 2009;118:115–30.
[6] Vinters HV. Cerebral amyloid angiopathy. In: Barnett HJM, Mohr JP, Stein BM, Yatsu FM, editors. Stroke pathophysiology, diagnosis and management. 2nd ed. New York: Churchill Livingstone; 1992. p. 821–58.
[7] Calhoun ME, Burgermeister P, Phinney AL, et al. Neuronal overexpression of mutant amyloid precursor protein results in prominent deposition of cerebrovascular amyloid. Proc Natl Acad Sci USA 1999;96:14088–93.
[8] Weller RO, Djuanda E, Yow HY, Carare RO. Lymphatic drainage of the brain and the pathophysiology of neurological disease. Acta Neuropathol 2009;117:1–14.
[9] Weller RO, Massey A, Newman TA, Hutchings M, Kuo YM, Roher AE. Cerebral amyloid angiopathy: amyloid beta accumulates in putative interstitial fluid drainage pathways in Alzheimer's disease. Am J Pathol 1998;153:725–33.
[10] Utter S, Tamboli IY, Walter J, et al. Cerebral small vessel disease-induced apolipoprotein E leakage is associated with Alzheimer disease and the accumulation of amyloid beta-protein in perivascular astrocytes. J Neuropathol Exp Neurol 2008;67:842–56.
[11] Grinberg LT, Thal DR. Vascular pathology in the aged human brain. Acta Neuropathol 2010;119:277–90.
[12] Thal DR. The pre-capillary segment of the blood-brain barrier and its relation to perivascular drainage in Alzheimer's disease and small vessel disease. ScientificWorldJournal 2009;9:557–63.
[13] Thal DR, Larionov S, Abramowski D, et al. Occurrence and co-localization of amyloid beta-protein and apolipoprotein E in perivascular drainage channels of wild-type and APP-transgenic mice. Neurobiol Aging 2007;28:1221–30.
[14] Bertram L, Tanzi RE. Thirty years of Alzheimer's disease genetics: the implications of systematic meta-analyses. Nat Rev Neurosci 2008;9:768–78.
[15] Corder EH, Saunders AM, Strittmatter WJ, et al. Gene dose of apolipoprotein E type 4 allele and the risk of Alzheimer's disease in late onset families. Science 1993;261:921–3.
[16] Thal DR, Ghebremedhin E, Rüb U, Yamaguchi H, Del Tredici K, Braak H. Two types of sporadic cerebral amyloid angiopathy. J Neuropathol Exp Neurol 2002;61:282–93.
[17] Attems J, Jellinger KA. Only cerebral capillary amyloid angiopathy correlates with Alzheimer pathology—a pilot study. Acta Neuropathol Berl 2004;107:83–90.
[18] Attems J, Lintner F, Jellinger KA. Amyloid beta peptide 1-42 highly correlates with capillary cerebral amyloid angiopathy and Alzheimer disease pathology. Acta Neuropathol Berl 2004;107:283–91.
[19] Thal DR, Griffin WS, Braak H. Parenchymal and vascular Abeta-deposition and its effects on the degeneration of neurons and cognition in Alzheimer's disease. J Cell Mol Med 2008;12:1848–62.
[20] Surbek B. L'angiopathie dyshorique (Morel) de l'écorce cérébrale. Etude anatomo-clinique et statistique, aspect génétique. Acta Neuropathol 1961;1:168–97.
[21] American Psychiatric Association. Diagnostic and statistical manual of mental disorders. 4th ed. Washington DC; 1994.
[22] The National Institute on Aging. Consensus recommendations for the postmortem diagnosis of Alzheimer's disease. The National Institute on Aging, and Reagan Institute Working Group on Diagnostic Criteria for the Neuropathological Assessment of Alzheimer's Disease. Neurobiol Aging 1997;18:S1–2.
[23] Insausti R, Amaral DG. Hippocampal formation. In: Paxinos G, Mai JK, editors. The human nervous system. 2nd edition. London: Elsevier; 2004. p. 872–914.
[24] Braak H, Braak E. Demonstration of amyloid deposits and neurofibrillary changes in whole brain sections. Brain Pathol 1991;1:213–6.
[25] Iqbal K, Braak H, Braak E, Grundke-Iqbal I. Silver labeling of Alzheimer neurofibrillary changes and brain beta-amyloid. J Histotechnol 1993;16:335–42.
[26] Alafuzoff I, Arzberger T, Al-Sarraj S, et al. Staging of neurofibrillary pathology in Alzheimer's disease. A study of the BrainNet Europe Consortium. Brain Pathol 2008;18:484–96.
[27] Braak H, Alafuzoff I, Arzberger T, Kretzschmar H, Del Tredici K. Staging of Alzheimer disease-associated neurofibrillary pathology using paraffin sections and immunocytochemistry. Acta Neuropathol 2006;112:389–404.
[28] Kim KS, Miller DL, Sapienza VJ, et al. Production and characterization of monoclonal antibodies reactive to synthetic cerebrovascular amyloid peptide. Neurosci Res Commun 1988;2:121–30.
[29] Braak H, Braak E. Neuropathological stageing of Alzheimer-related changes. Acta Neuropathol 1991;82:239–59.
[30] Mirra SS, Heyman A, McKeel D, et al. The Consortium to Establish a Registry for Alzheimer's Disease (CERAD). Part II. Standardization of the neuropathologic assessment of Alzheimer's disease. Neurology 1991;41:479–86.
[31] Thal DR, Rüb U, Schultz C, et al. Sequence of Abeta-protein deposition in the human medial temporal lobe. J Neuropathol Exp Neurol 2000;59:733–48.
[32] Thal DR, Rüb U, Orantes M, Braak H. Phases of Abeta-deposition in the human brain and its relevance for the development of AD. Neurology 2002;58:1791–800.
[33] Vonsattel JP, Myers RH, Hedley-Whyte ET, Ropper AH, Bird ED, Richardson Jr EP. Cerebral amyloid angiopathy without and with cerebral hemorrhages: a comparative histological study. Ann Neurol 1991;30:637–49.
[34] Bechmann I, Galea I, Perry VH. What is the blood-brain barrier (not)? Trends Immunol 2007;28:5–11.

[35] Yamaguchi H, Sugihara S, Ogawa A, Saido TC, Ihara Y. Diffuse plaques associated with astroglial amyloid beta protein, possibly showing a disappearing stage of senile plaques. Acta Neuropathol Berl 1998;95:217–22.
[36] Saido TC, Iwatsubo T, Mann DM, Shimada H, Ihara Y, Kawashima S. Dominant and differential deposition of distinct beta-amyloid peptide species, A beta N3(pE), in senile plaques. Neuron 1995;14:457–66.
[37] Tekirian TL, Saido TC, Markesbery WR, et al. N-terminal heterogeneity of parenchymal and cerebrovascular Abeta deposits. J Neuropathol Exp Neurol 1998;57:76–94.
[38] Lalowski M, Golabek A, Lemere CA, et al. The "nonamyloidogenic" p3 fragment (amyloid beta17–42) is a major constituent of Down's syndrome cerebellar preamyloid. J Biol Chem 1996;271:33623–31.
[39] Thal DR, Sassin I, Schultz C, Haass C, Braak E, Braak H. Fleecy amyloid deposits in the internal layers of the human entorhinal cortex are comprised of N-terminal truncated fragments of Abeta. J Neuropathol Exp Neurol 1999;58:210–6.
[40] Lemere CA, Blusztajn JK, Yamaguchi H, Wisniewski T, Saido TC, Selkoe DJ. Sequence of deposition of heterogeneous amyloid beta-peptides and APO E in Down syndrome: implications for initial events in amyloid plaque formation. Neurobiol Dis 1996;3:16–32.
[41] Iwatsubo T, Saido TC, Mann DM, Lee VM, Trojanowski JQ. Full-length amyloid-beta (1–42(43)) and amino-terminally modified and truncated amyloid-beta 42(43) deposit in diffuse plaques. Am J Pathol 1996;149:1823–30.
[42] Thal DR, Capetillo-Zarate E, Schultz C, et al. Apolipoprotein E co-localizes with newly formed amyloid beta-protein (Abeta)-deposits lacking immunoreactivity against N-terminal epitopes of Abeta in a genotype-dependent manner. Acta Neuropathol 2005;110:459–71.
[43] Dickson DW, Farlo J, Davies P, Crystal H, Fuld P, Yen SH. Alzheimer's disease. A double-labeling immunohistochemical study of senile plaques. Am J Pathol 1988;132:86–101.
[44] Thal DR, Hartig W, Schober R. Diffuse plaques in the molecular layer show intracellular A beta(8–17)- immunoreactive deposits in subpial astrocytes. Clin Neuropathol 1999;18:226–31.
[45] Thal DR, Schultz C, Dehghani F, Yamaguchi H, Braak H, Braak E. Amyloid beta-protein (Abeta)-containing astrocytes are located preferentially near N-terminal-truncated Abeta deposits in the human entorhinal cortex. Acta Neuropathol Berl 2000;100:608–17.
[46] Kumar-Singh S, Pirici D, McGowan E, et al. Dense-core plaques in Tg2576 and PSAPP mouse models of Alzheimer's disease are centered on vessel walls. Am J Pathol 2005;167:527–43.
[47] Thal DR, Papassotiropoulos A, Saido TC, et al. Capillary cerebral amyloid angiopathy identifies a distinct APOE epsilon4-associated subtype of sporadic Alzheimer's disease. Acta Neuropathol 2010;120:169–83.
[48] Thal DR, Griffin WST, De Vos RAI, Ghebremedhin E. Cerebral amyloid angiopathy and its relationship to Alzheimer's disease. Acta Neuropathol 2008;115:599–609.
[49] Deane R, Sagare A, Hamm K, et al. apoE isoform-specific disruption of amyloid beta peptide clearance from mouse brain. J Clin Invest 2008;118:4002–13.
[50] Bruinsma IB, Wilhelmus MM, Kox M, Veerhuis R, de Waal RM, Verbeek MM. Apolipoprotein E protects cultured pericytes and astrocytes from D-Abeta(1–40)-mediated cell death. Brain Res 2010;1315:169–80.
[51] Olichney JM, Hansen LA, Hofstetter CR, Lee JH, Katzman R, Thal LJ. Association between severe cerebral amyloid angiopathy and cerebrovascular lesions in Alzheimer disease is not a spurious one attributable to apolipoprotein E4. Arch Neurol 2000;57:869–74.
[52] Cortes-Canteli M, Paul J, Norris EH, et al. Fibrinogen and beta-amyloid association alters thrombosis and fibrinolysis: a possible contributing factor to Alzheimer's disease. Neuron 2010;66:695–709.
[53] Mazur-Kolecka B, Dickson D, Frackowiak J. Induction of vascular amyloidosis-beta by oxidative stress depends on APOE genotype. Neurobiol Aging 2006;27:804–14.
[54] Mazur-Kolecka B, Frackowiak J, Carroll RT, Wisniewski HM. Accumulation of Alzheimer amyloid-beta peptide in cultured myocytes is enhanced by serum and reduced by cerebrospinal fluid. J Neuropathol Exp Neurol 1997;56:263–72.
[55] Alafuzoff I, Adolfsson R, Grundke-Iqbal I, Winblad B. Blood-brain barrier in Alzheimer dementia and in non-demented elderly. An immunocytochemical study. Acta Neuropathol 1987;73:160–6.
[56] Ishii T, Haga S, Shimizu F. Identification of components of immunoglobulins in senile plaques by means of fluorescent antibody technique. Acta Neuropathol 1975;32:157–62.
[57] Cullen KM, Kocsi Z, Stone J. Microvascular pathology in the aging human brain: evidence that senile plaques are sites of microhaemorrhages. Neurobiol Aging 2006;27:1786–96.
[58] Pfeifer M, Boncristiano S, Bondolfi L, et al. Cerebral hemorrhage after passive anti-Abeta immunotherapy. Science 2002;298:1379.
[59] Kimberly WT, Gilson A, Rost NS, et al. Silent ischemic infarcts are associated with hemorrhage burden in cerebral amyloid angiopathy. Neurology 2009;72:1230–5.
[60] Koistinaho M, Lin S, Wu X, et al. Apolipoprotein E promotes astrocyte colocalization and degradation of deposited amyloid-beta peptides. Nat Med 2004;10:719–26.
[61] Yamaguchi H, Yamazaki T, Lemere CA, Frosch MP, Selkoe DJ. Beta amyloid is focally deposited within the outer basement membrane in the amyloid angiopathy of Alzheimer's disease. An immunoelectron microscopic study. Am J Pathol 1992;141:249–59.

Journal of Neuroscience Research

Journal of Neuroscience Research 88:3588–3597 (2010)

Efficient Four-Drug Cocktail Therapy Targeting Amyloid-β Peptide for Alzheimer's Disease

Masashi Asai,[1,2]* Nobuhisa Iwata,[2] Taisuke Tomita,[3,4] Takeshi Iwatsubo,[3,4,5] Shoichi Ishiura,[6] Takaomi C. Saido,[2] and Kei Maruyama[1]

[1]Department of Pharmacology, Faculty of Medicine, Saitama Medical University, Saitama, Japan
[2]Laboratory for Proteolytic Neuroscience, RIKEN Brain Science Institute, Saitama, Japan
[3]Department of Neuropathology and Neuroscience, Graduate School of Pharmaceutical Sciences, The University of Tokyo, Tokyo, Japan
[4]Core Research for Evolutional Science and Technology (CREST), Japan Science and Technology Corporation, Tokyo, Japan
[5]Department of Neuropathology, Graduate School of Medicine, The University of Tokyo, Tokyo, Japan
[6]Department of Life Sciences, Graduate School of Arts and Sciences, The University of Tokyo, Tokyo, Japan

Cocktail treatment is an effective multidrug medication therapy for some diseases, such as cancer and AIDS, because of the additive or synergistic effect of each medicine and relief from adverse effects. Amyloid-β peptide (Aβ), which is now recognized as central to the development of Alzheimer's disease (AD), is derived from the sequential proteolysis of amyloid precursor protein (APP) by β- and γ-secretases. Secretase inhibitors are one of most attractive targets for therapeutic intervention in AD. However, because β- and γ-secretases cleave not only APP but also other substrate proteins, strong inhibition of these secretases leads to severe adverse effects. Some nonsteroidal antiinflammatory drugs (NSAIDs) and cholesterol-lowering drugs (statins) can modify the production of Aβ. Here, we report that a cocktail treatment with four drugs (NSAID, statin, and β- and γ-secretase inhibitors) had additive effects on the reduction of Aβ levels in cultured cells without competing with each other. Moreover, the four-drug cocktail treatment caused no changes in processing of the γ-secretase substrate Notch. This is suggests that this cocktail treatment could be a new therapeutic approach for AD.

Key words: NSAID; β-secretase inhibitor; γ-secretase inhibitor; statin; cocktail therapy

Alzheimer's disease (AD) is the most frequent type of elderly dementia. It is characterized by the deposition of amyloid plaques, accumulation of neurofibrillary tangles, and loss of neurons and synapses in particular areas of the brain (Selkoe, 2002; Mattson, 2004). AD occurs in both sporadic and familial forms, with generally similar pathology according to the amyloid hypothesis, which is based on the metabolic imbalance between the production and clearance of amyloid-β peptide (Aβ; Iwata et al., 2005; Blennow et al., 2006). Aβ is derived from the sequential proteolysis of amyloid precursor protein (APP) by β- and γ-secretases (Mattson, 2004; Blennow et al., 2006) and plays a critical role in AD pathogenesis. Therefore, lowering Aβ levels in the brain serves as a disease-modifying therapy for AD.

Because inhibitors of β- and γ-secretases directly block Aβ production, they are promising and attractive therapeutic targets for AD (Mattson, 2004; Marks and Berg, 2008). Indeed, many compounds have been developed that inhibit these secretases and reduce Aβ levels in vitro and in vivo (Stachel et al., 2004; Wong et al. 2004; Asai et al., 2006). However, because β- and γ-secretases act on a variety of substrates, type I membrane proteins, in addition to APP (Marks and Berg, 2008), it has been suggested that strong inhibition of their protease activity may produce adverse effects (De Strooper et al., 1999; Geling et al., 2002; Wong et al., 2004; Dominguez et al., 2005; Willem et al., 2006).

Some nonsteroidal antiinflammatory drugs (NSAIDs) and widely used cholesterol-lowering drugs (statins) are also capable of reducing Aβ levels (Fassbender et al., 2001; Weggen et al., 2001; Eriksen et al., 2003). Statins, 3-hydroxy-3-methylglutaryl-CoA (HMG-CoA) reductase inhibitors, suppress Aβ production and activate the alter-

Contract grant sponsor: Grant-in-Aid for Young Scientists (19790194) from Japan Society for the Promotion of Science (JSPS) (to M.A.); Contract grant sponsor: Grant-in-Aid for Scientific Research (20590260) from Japan Society for the Promotion of Science (JSPS) (to K.M.); Contract grant sponsor: Ochiai Memorial Award 2004 (to M.A.).

*Correspondence to: Masashi Asai, 38 Moro-hongo, Moroyama-machi, Iruma-gun, Saitama 350-0495, Japan. E-mail: asai@saitama-med.ac.jp

Received 20 January 2010; Revised 13 July 2010; Accepted 1 August 2010

Published online 1 October 2010 in Wiley Online Library (wileyonlinelibrary.com). DOI: 10.1002/jnr.22503

nate pathway for APP metabolism, the nonamyloidogenic α-secretase pathway (Fassbender et al., 2001). Several NSAIDs, including sulindac sulfide, modulate γ-secretase activity, thereby decreasing the secretion of Aβ42, which is more prone to aggregation than Aβ40 and is predominantly deposited in AD brains, but show little effect on the secretion of Aβ40 (Weggen et al., 2001). Almost all familial AD-linked mutations of causal genes, such as APP and presenilin (PS) 1 and 2, promote the production of Aβ42 and elevate the Aβ42-to-Aβ40 ratio (Aβ42/Aβ40), accelerating AD pathogenesis (Wolfe, 2007). Thus, NSAIDs are potential disease-modifying agents for AD, although a relatively high dose is required for this effect (Blennow et al., 2006; Weggen et al., 2007).

Although the removal of Aβ from the brain is required for treatment of AD, there are, currently, no fundamental therapeutic drugs targeting Aβ (Saido and Iwata, 2006; Marks and Berg, 2008). Indeed, the sole use of secretase inhibitors at a high dose is likely to cause adverse effects. However, a cocktail treatment (a combination of 2–4 drugs) at relatively low doses (e.g., 20–30% efficacies in each case) would give rise to an additive or synergistic effect and alleviate the adverse effects (Saido and Iwata, 2006). There is much evidence suggesting that there are multiple strategies to reduce Aβ levels, so we designed a combinatorial approach targeting different processes in the production of Aβ. Inhibition of Aβ production prevents AD development via formation of particular forms of Aβ, such as Aβ oligomers. The drug cocktail consisted of β- and γ-secretase inhibitors, an NSAID, and a statin. Here, we report that this four-drug cocktail was remarkably effective in reducing Aβ levels without competing with each other or causing apparent adverse effects. It is suggested that this four-drug cocktail is a new and potentially powerful approach to the treatment of AD.

MATERIALS AND METHODS

Reagents and Antibodies

The β-secretase inhibitor IV (*N*-[(1*S*, 2*R*)-1-benzyl-3-(cyclopropylamino)-2-hydroxypropyl]-5-[methyl(methylsulfonyl) amino-*N'*-[(1*R*)-1-phenylethyl]isophthalamide; Stachel et al., 2004), γ-secretase inhibitor XXI (also known as "compound E"; (*S,S*)-2-[2-(3,5-difluorophenyl)-acetylamino]-*N*-(1-methyl-2-oxo-5-phenyl-2,3-dihydro-1H-benzo[e][1,4]diazepin-3-yl)-propionamide; Seiffert et al., 2000), and the sodium salt of simvastatin were purchased from Merck KGaA (Darmstadt, Germany); sulindac sulfide was purchased from Sigma-Aldrich (St. Louis, MO). All drugs were dissolved in sterilized dimethyl sulfoxide (DMSO) and added to cell culture medium to give a final concentration of 0.1% DMSO. Monoclonal antibody 22C11 (Chemicon, Temecula, CA), which recognizes amino acid residues 66–81 at the N-terminus of APP, was used at a concentration of 1:1,000. Monoclonal antibody 2B3 (Immuno-Biological Laboratories Co., Gunma, Japan), which recognizes amino acid residues at the C-terminal end of human soluble extracellular fragment of APP generated by α-secretase (sAPPα), was used at a concentration of 2 μg/ml. The polyclonal anti-sAPPβ$_{NL}$ antibody was used at a concentration of 1:1,000 to detect the soluble extracellular fragment of APPsw (APP with Swedish mutation) generated by β-secretase (sAPPβ), as previously described (Asai et al., 2007). Monoclonal antibody 82E1 (Immuno-Biological Laboratories Co.), which recognizes amino acid residues 1–16 of the human Aβ sequence, was used at 1 μg/ml. Polyclonal anti-APP antibody (catalogue No. A8717; Sigma-Aldrich), which recognizes amino acid residues 676–695 at the C-terminus of APP$_{695}$, was used at a concentration of 1:15,000. Monoclonal antibody AC-74 (Sigma-Aldrich), which recognizes amino acid residues at the N-terminal end of β-actin, was used at a concentration of 1:5,000. Monoclonal antibody 9B11 (Cell Signaling Technology, Danvers, MA), which recognizes the myc epitope tag (corresponding to amino acid residues 410–419 of human c-Myc), was used at a concentration of 1:1,000.

Cell Culture

An expression vector encoding mouse Notch deleted extracellular domain (mNotch$^{\Delta E}$) in pCS2 (Kopan et al., 1996) was provided by Dr. Raphael Kopan (Washington University). An expression vector encoding enhanced green fluorescent protein (EGFP) was digested from pEGFP-N1 (BD Biosciences Clontech Laboratories, Palo Alto, CA) and subcloned into the pcDNA3 vector (Invitrogen, Carlsbad, CA; Imamura et al., 2009). A stable Neuro2a (N2a) cell line (mNotch$^{\Delta E}$-N2a cells) doubly expressing mNotch$^{\Delta E}$ and EGFP and a stable H4 cell line (APP$_{NL}$-H4 cells) stably expressing human APP$_{695}$ with the Swedish mutation (Asai et al, 2007) were cultured in Dulbecco's modified Eagle's medium (DMEM; Invitrogen) at 37°C in 5% CO_2. DMEM was supplemented with 10% fetal bovine serum (BioWest, Nuaillé, France), 100 U/ml penicillin, 100 μg/ml streptomycin (Invitrogen), and 160 μg/ml G418 (Merck KGaA) for mNotch$^{\Delta E}$-N2a cells or 150 μg/ml hygromycin B (Wako Pure Chemical Industries Ltd., Osaka, Japan) for APP$_{NL}$-H4 cells. Cells were grown for 24 hr in a 24-well plate or a 6-cm dish. The drugs were then added to the conditioned culture medium, and the cells were incubated for 24 hr. Both conditioned media were supplemented with lipid-free serum (BioWest).

Cell Toxicity Analysis

Cell toxicity assay was assessed with a cytotoxicity detection kit (Roche Diagnostics GmbH, Mannheim, Germany) that determines the amount of lactate dehydrogenase (LDH) released into the cell culture medium from dying cells.

Aβ Sandwich ELISA

Extracellular Aβ40 and Aβ42 levels in the conditioned media from cultured mNotch$^{\Delta E}$-N2a or APP$_{NL}$-H4cells were measured by an Aβ enzyme-linked immunosorbent assay (ELISA) kit (Wako Pure Chemical Industries Ltd.).

Western Blot Analysis

Cells treated with drugs were harvested and lysed in a buffer containing 10 mM HEPES (pH 7.4), 150 mM NaCl, 0.5% Triton X-100, and protease inhibitor cocktail (Roche

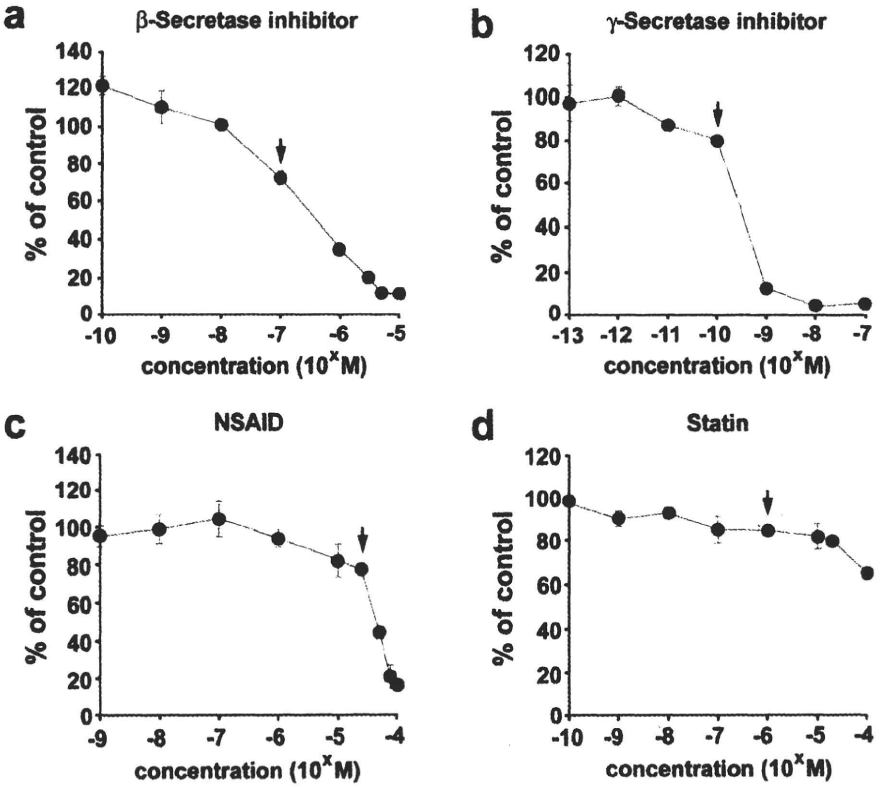

Fig. 1. Determination of the concentration of each single drug for the cocktail treatment. Amount of Aβ42 released into the conditioned medium from APP_{NL}-H4 cells treated with each drug was measured by sandwich ELISA β-secretase inhibitor (**a**), γ-secretase inhibitor (**b**), NSAID (**c**), and statin (**d**). Data represent the mean ± SD of three experiments. Actual values of Aβ40 and Aβ42 concentrations in the control group (vehicle treatment) are 1,861 ± 168 pM and 58.3 ± 7.2 pM, respectively. Each arrow indicates the concentrations for which the combinational drug experiments shown in Figures 2–5 were performed.

Applied Science) on ice. The cell lysate was freeze-thawed three times at 20-min intervals and centrifuged at 13,000*g* for 15 min at 4°C. The supernatant protein concentrations were determined using a BCA protein assay kit (Pierce Biotechnology, Rockford, IL).

sAPP secreted into the conditioned media was precipitated with heparin agarose resin (Pierce Biotechnology). Equal amounts of proteins in the cell lysates or sAPP collected from equal volumes of conditioned media were subjected to sodium dodecyl sulfate-polyacrylamide gel electrophoresis, and the proteins in the gels were transferred to polyvinylidene difluoride membranes (Hybond-P; GE Healthcare UK, Buckinghamshire, United Kingdom) or nitrocellulose transfer membrane (Protran; Whatman GmbH, Dassel, Germany). The membranes were probed with an appropriate primary antibody and then treated with an appropriate secondary antibody, namely, horseradish peroxidase-conjugated anti-mouse or anti-rabbit IgG (GE Healthcare UK). The protein bands were visualized using an enhanced chemiluminescence (ECL) detection method (GE Healthcare UK), and band intensity was analyzed with a densitometer (LAS-4000; Fujifilm Corporation, Tokyo, Japan), using the Science Laboratory 2001 Image Gauge software (Fujifilm Corporation).

Statistical Analysis

All values were expressed as the mean ± SD. For comparisons of two groups, a two-tailed Student's *t*-test was used. For comparisons among more than three groups, Dunnett's or SNK multiple-comparisons tests were used. A difference was considered significant at $P < 0.05$.

RESULTS

Determination of Single Doses of Drugs

We selected the most potent compounds for the β- and γ-secretase inhibitors, NSAID, and statin from commercially available reagents; we used the β-secretase inhibitor IV (Stachel et al., 2004), γ-secretase inhibitor XXI/compound E (Seiffert et al., 2000), sulindac sulfide (Weggen et al., 2001), and simvastatin (Fassbender et al., 2001). We first evaluated the inhibitory effect of each drug on Aβ42 production (Fig. 1). All of these drugs inhibited production of Aβ42, whose secretion from APP_{NL}-H4 cells was decreased in a dose-dependent manner. On the basis of these results, we selected a dose for each drug with an approximately 15–30% inhibitory

effect on Aβ42 production: β-secretase inhibitor, 100 nM (% of inhibition on Aβ42 production = 27.7%); γ-secretase inhibitor, 100 pM (19.5%); NSAID, 25 μM (23%); and statin, 1 μM (15.5%); as indicated by the arrows in Figure 1. We also confirmed that these doses had no significant effect on LDH release compared with the vehicle treatment (Table I).

TABLE I. Effect of Single Drug or Cocktail Administration on Cell Toxicity*

Reagent	LDH release (% of control)
Vehicle	100.0 ± 3.7
β-Secretase inhibitor	90.9 ± 6.4
γ-Secretase inhibitor	92.2 ± 6.8
NSAID	92.2 ± 5.0
Statin	105.0 ± 8.1
Cocktail	109.1 ± 13.4

*APP_{NL}-H4 cells were treated with the indicated reagent for 24 hr, and cell toxicity was assessed by the LDH assay. Data are the mean ± SD of nine experiments in each group.

Combinatorial Effects of the β-Secretase Inhibitor With One of the Other Drugs on Aβ Production

We next examined both Aβ40 and Aβ42 levels in the conditioned media from APP_{NL}-H4 cells treated with the γ-secretase inhibitor, NSAID, or statin, in the presence of the β-secretase inhibitor (Fig. 2). The administration of each drug in combination with the β-secretase inhibitor significantly reduced Aβ40 levels at low doses of the β-secretase inhibitor compared with administration of the β-secretase inhibitor alone (Fig. 2a). However, at a high concentration of the β-secretase inhibitor, a significant cooperative effect on Aβ40 levels was not observed (Fig. 2a). The β-secretase inhibitor showed a significant reduction in Aβ42 levels only at doses of 10^{-9} and 10^{-8} M in combination with the γ-secretase inhibitor, whereas the NSAID and statin

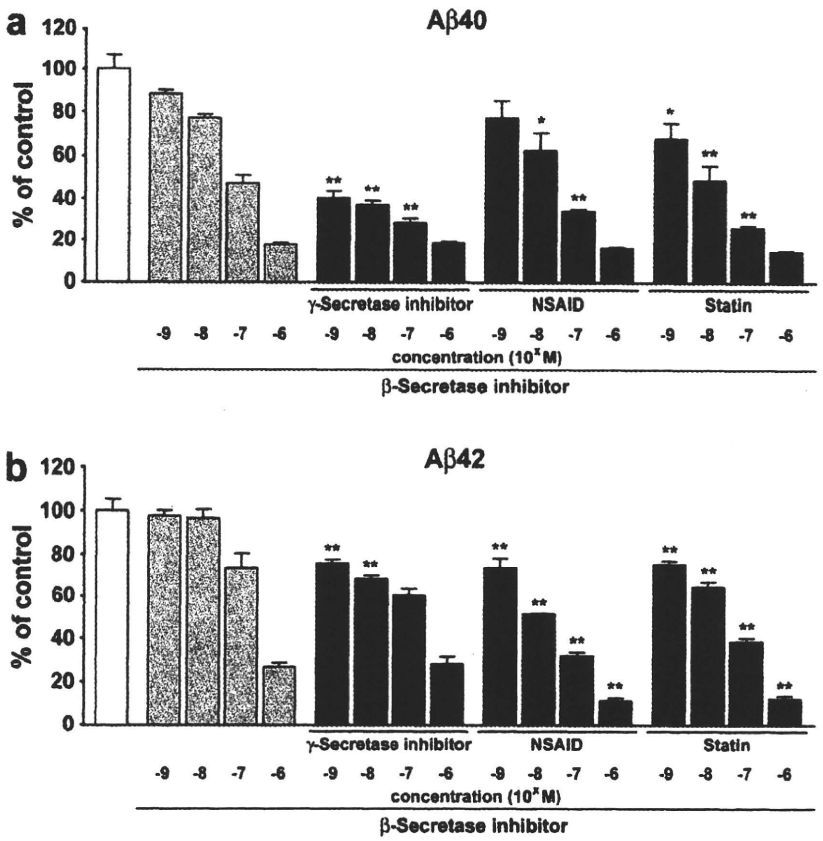

Fig. 2. Effect of the combination of the β-secretase inhibitor with the other drugs on Aβ40 and Aβ42 levels. Amount of Aβ released into the conditioned medium from APP_{NL}-H4 cells treated with each drug in the presence of the β-secretase inhibitor was measured by sandwich ELISA. Doses of the γ-secretase inhibitor, NSAID, and statin were 100 pM, 25 μM, and 1 μM, respectively. Levels of Aβ are expressed as Aβ40 (**a**) and Aβ42 (**b**). Data represent the mean ± SD of three experiments. $*P < 0.05$, $**P < 0.01$, significantly different from the group treated with the β-secretase inhibitor alone at the corresponding concentration.

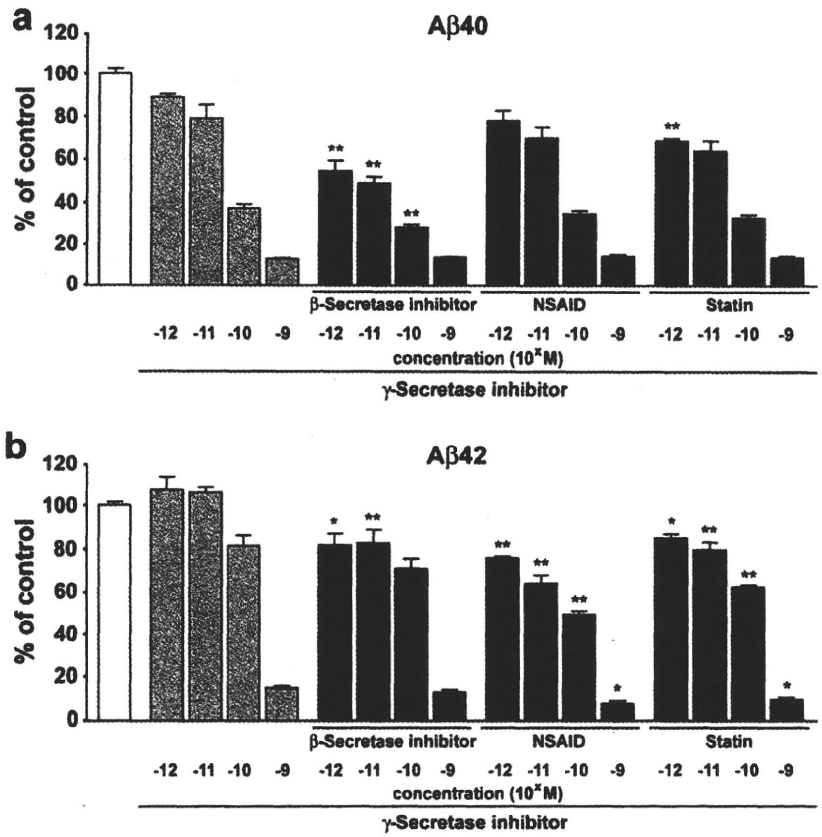

Fig. 3. Effect of the combination of γ-secretase inhibitor with the other drugs on Aβ40 and Aβ42 levels. Amount of Aβ released into the conditioned medium from APP_{NL}-H4 cells treated with each drug in the presence of the γ-secretase inhibitor was measured by sandwich ELISA. Doses of the β-secretase inhibitor, NSAID, and statin were 100 nM, 25 μM, and 1 μM, respectively. Levels of Aβ are expressed as Aβ40 (**a**) and Aβ42 (**b**). Data represent the mean ± SD of three experiments. $*P < 0.05$, $**P < 0.01$, significantly different from group treated with the γ-secretase inhibitor alone at the corresponding concentration.

reduced Aβ42 levels at all doses of the β-secretase inhibitor (Fig. 2b).

Combinatorial Effects of γ-Secretase Inhibitor With One of the Other Drugs on Aβ Production

We examined both Aβ40 and Aβ42 levels in the conditioned media of APP_{NL}-H4 cells treated with the β-secretase inhibitor, NSAID, or statin, in the presence of the γ-secretase inhibitor (Fig. 3). The combinatorial administration of the two secretase inhibitors effectively reduced Aβ40 levels at 10^{-9} to 10^{-6} M of the γ-secretase inhibitor compared with administration of the γ-secretase inhibitor alone (Fig. 3a). At all doses of the γ-secretase inhibitor, however, the NSAID or statin had no additional effects on Aβ40 levels (Fig. 3a). However, these combinations significantly reduced the level of Aβ42 at 10^{-9} to 10^{-6} M of the γ-secretase inhibitor compared with administration of the γ-secretase inhibitor alone (Fig. 3b).

Comparison of the Effects on Aβ Production and the Aβ42/Aβ40 Ratio Between Each Drug and the Four-Drug Cocktail

To assess whether the four-drug cocktail suppressed Aβ production more than each drug alone, we measured the Aβ40 and Aβ42 levels in the conditioned media from APP_{NL}-H4 cells treated with each drug alone or the four-drug cocktail (Fig. 4a–c). The four-drug cocktail acted additively to reduce Aβ40 and Aβ42 levels (Aβ40 level = 23.8% ± 0.6%, Aβ42 level = 28.3% ± 2.8%) with no change in the Aβ ratio (Aβ42/Aβ40 = 118.4% ± 11.7%) compared with the vehicle-treated group (Fig. 4a–c); the observed effects were more prominent than for each drug alone. The β- or γ-secretase inhibitor alone significantly decreased both Aβ40 and Aβ42 levels (β-secretase inhibitor: Aβ40 level = 48.0% ± 5.3%, Aβ42 level = 61.4% ± 7.7%; γ-secretase inhibitor: Aβ40 level = 50.1% ± 9.2%, Aβ42 level = 77.4% ± 9.4%), but they increased the Aβ42/Aβ40 ratio (β-secretase inhibitor: Aβ42/Aβ40 = 127.3% ±

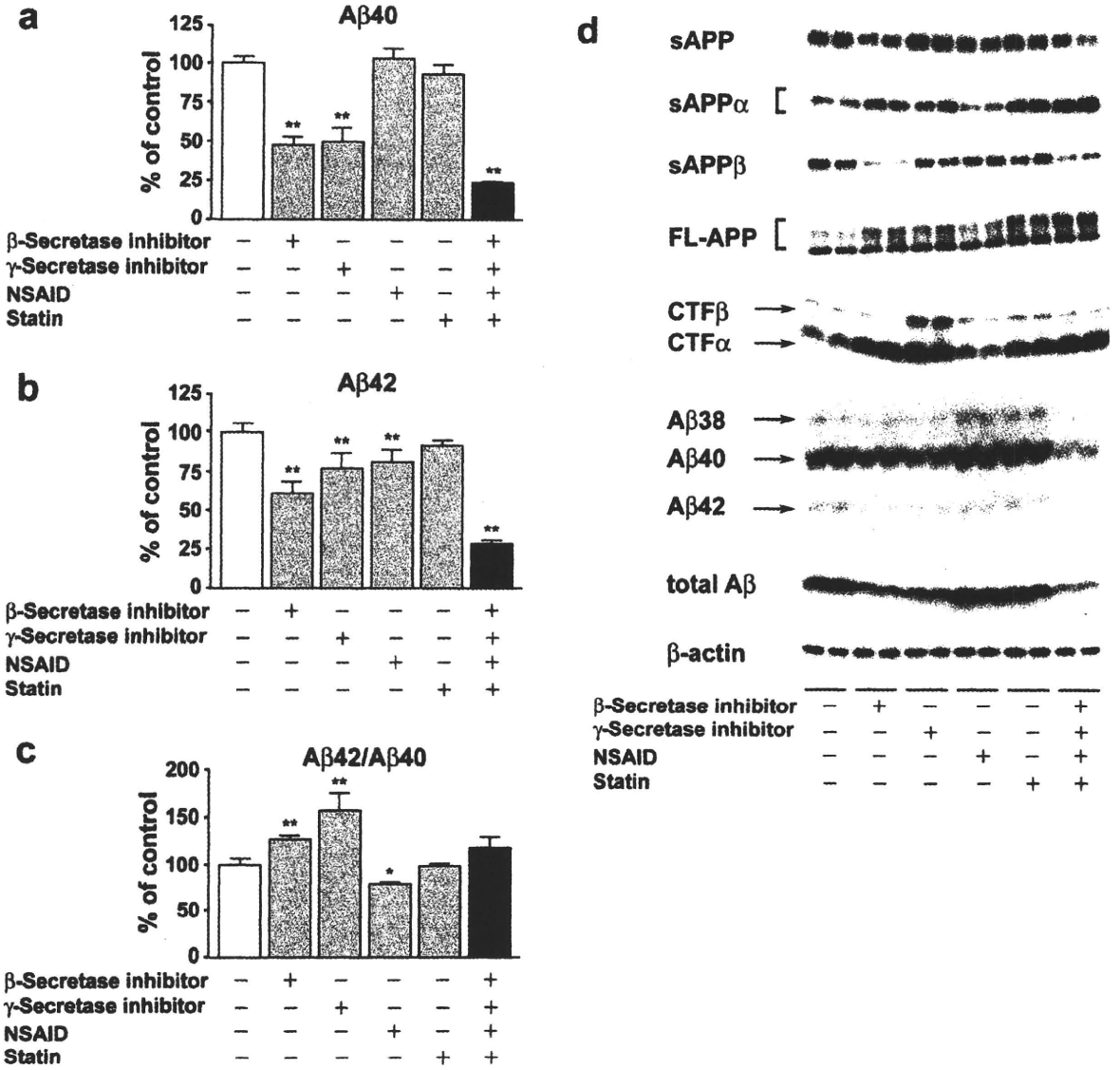

Fig. 4. Comparison of the effects on Aβ production and the Aβ42/Aβ40 ratio for each drug and the four-drug cocktail. Amount of Aβ released into the conditioned medium from APP_{NL}-H4 cells treated with each drug or the four-drug cocktail was measured by sandwich ELISA (a–c). Aβ levels and the Aβ42/Aβ40 ratio are expressed as Aβ40 (**a**), Aβ42 (**b**), and Aβ42/Aβ40 (**c**). Data represent the mean ± SD of four experiments. $*P < 0.05$, $**P < 0.01$, significantly different from the vehicle-treated group (a–c). Results of Western blot analysis for sAPP, sAPPα, sAPPβ, FL-APP, CTFα, CTFβ, Aβ species, total Aβ, and β-actin are shown in **d**. FL, full-length; CTF, C-terminal fragment.

3.8%; γ-secretase inhibitor: Aβ42/Aβ40 = 156.9% ± 18.2%) compared with the vehicle-treated group (Fig. 4a–c). Western blot analysis showed that the four-drug cocktail treatment caused effective decreases in Aβ40, Aβ42, and total Aβ levels and a corresponding increase in sAPPα (Fig. 4d). The four-drug cocktail treatment had no significant effect on cytotoxicity in APP_{NL}-H4 cells (Table I).

Comparison Between the γ-Secretase Inhibitor and Four-Drug Cocktail in Notch Processing and Aβ Levels

γ-Secretase is involved in the intracellular proteolysis of a range of substrates (Beel and Sanders, 2008). Although its inhibitors effectively block Aβ production in vivo and in vitro (Shearman et al., 2000; Beher et al., 2001), they also inhibit the processing of substrate